

Spectator Interactions in $B \rightarrow V\gamma$ Decays and QCD Factorisation

S. Descotes-Genon^a and C.T. Sachrajda^b

^a *Laboratoire de Physique Théorique¹, Université Paris XI
91405 Orsay Cedex, France*

^b *School of Physics and Astronomy, Univ. of Southampton,
Southampton, SO17 1BJ, United Kingdom*

Abstract

We study the radiative decays $B \rightarrow V\gamma$ (where $V = \rho, K^*$) in the framework of QCD factorisation, and in particular the hard-spectator contributions to the decay amplitudes. For the phenomenologically significant chromomagnetic operator, we show by an explicit next-to-leading-order computation that the spectator interactions factorise in the heavy-quark limit, i.e. that they can be written as the convolution of a hard-scattering kernel, computable in perturbation theory, and of the light-cone distribution amplitudes for the B and V mesons which contain the soft physics. The presence of an intermediate scale of $O(M_B\Lambda_{\text{QCD}})$ leads to the presence of Sudakov logarithms. We indicate how the demonstration of factorisation can be extended to other (four-quark) operators.

PACS numbers: 12.38.Bx, 12.39.Hg, 12.39.St, 13.25.Hw

¹LPT is an Unité Mixte de Recherche du CNRS et de l'Université Paris XI (UMR 8627)

1 Introduction

Radiative $B \rightarrow V\gamma$ decays (where V is a light vector meson) are processes of particular interest in flavour physics which are already accessible at B -factories. Current measurements yield the following branching ratios [1]:

$$B(B^0 \rightarrow K^{*0}\gamma) = (4.18 \pm 0.23) \cdot 10^{-5} \quad B(B^+ \rightarrow K^{*+}\gamma) = (4.14 \pm 0.33) \cdot 10^{-5},$$

whereas only upper bounds are available for the $\omega^0\gamma$, $\rho^0\gamma$ and $\rho^+\gamma$ modes (of order $O(10^{-6})$ at 90 % confidence level) [2]. Within the standard model these decays can give measurements of the V_{td} and V_{ts} elements of the CKM matrix.

Penguin-mediated processes, such as $b \rightarrow s\gamma$ and $b \rightarrow d\gamma$ radiative decays, exhibit particular sensitivity to physics beyond the standard model. It is therefore theoretically important to be able to disentangle the Standard Model contributions from potential effects of new physics. The principal difficulty in calculating the amplitudes is due to the presence of non-perturbative QCD effects. For inclusive decays, such as $B \rightarrow X_s\gamma$, an operator product expansion allows the decay amplitude to be computed as a series in inverse powers of m_b (the mass of the b -quark), with the leading term being calculable in perturbation theory [3]. For exclusive decays the decay amplitudes can be calculated in the framework of QCD factorisation, first developed for nonleptonic two-body decays [4, 5]. At leading order in $1/M_B$, the long-distance QCD effects are factorised into universal quantities, the $B \rightarrow$ meson transition form factors and the light-cone distribution amplitudes of the mesons.

The factorisation framework has been applied to $B \rightarrow K^*\gamma$ and $B \rightarrow \rho\gamma$ decays, refs. [6, 7], where in addition to the leading-twist contributions, the subleading (but phenomenologically relevant) effects of weak annihilation were also considered. The same class of decays was also analysed in an effective-theory framework at higher orders in perturbation theory [8]. The subsequent phenomenological analysis suggests interesting quantities to constrain the shape of the unitarity triangle, such as the $\rho\gamma$ CP-asymmetry for the γ angle [6] and the ratio of branching ratios for $\rho^0\gamma$ and $K^{*0}\gamma$ for the R_t side (which provides bounds already competitive with the $B - \bar{B}$ and $B_s - \bar{B}_s$ mass differences) [9]. These flavour-changing neutral-current processes yield strong constraints on supersymmetric models [10].

In view of their phenomenological importance, $B \rightarrow V\gamma$ decays deserve further investigation in the framework of QCD factorisation. In this paper we focus on (strong) radiative corrections to spectator interactions, in order to determine whether and how factorisation holds at higher orders in perturbation theory. We have previously followed a similar line of investigation for the purely radiative decay $B \rightarrow \gamma\ell\nu$ [11] (and the related decays $B \rightarrow \gamma\gamma$ and $B \rightarrow \gamma\ell^+\ell^-$ [12]) in order to acquire a better understanding of the properties of the light-cone distribution amplitude of the B -meson. $B \rightarrow V\gamma$ decays provide an opportunity to study similar issues concerning the factorisation of long-distance effects, but now with the presence of a hadron in the final state. In addition, these decays possess similar features to heavy-to-light semileptonic decays, such as $B \rightarrow \pi\ell\nu$ which are currently being studied in the SCET framework [13, 14] (see refs. [15, 16, 17] for recent progress).

The effective Hamiltonian for $B \rightarrow V\gamma$ decays, where V is a light-vector meson V is [18]:

$$\mathcal{H} = \frac{G_F}{\sqrt{2}} \sum_{p=u,c} \lambda_p^{(q)} [C_1 \mathcal{Q}_1^p + C_2 \mathcal{Q}_2^p + \sum_{i=3}^8 C_i \mathcal{Q}_i] \quad (1)$$

where $\lambda_p^{(q)} = V_{pq}^* V_{pb}$ (unitarity of the CKM matrix implies that $\lambda_t^{(q)} = -(\lambda_u^{(q)} + \lambda_c^{(q)})$) and so contributions from diagrams with loops containing a top quark are included implicitly). $\mathcal{Q}_1 - \mathcal{Q}_6$ are four-quark operators:

$$\mathcal{Q}_1^p = (\bar{q}p)_{V-A} (\bar{p}b)_{V-A} \quad \mathcal{Q}_2^p = (\bar{q}_i p_j)_{V-A} (\bar{p}_j b_i)_{V-A} \quad (2)$$

$$\mathcal{Q}_3 = (\bar{q}b)_{V-A} \sum_{q'} (\bar{q}' q')_{V-A} \quad \mathcal{Q}_4 = (\bar{q}_i b_j)_{V-A} \sum_{q'} (\bar{q}'_j q'_i)_{V-A} \quad (3)$$

$$\mathcal{Q}_5 = (\bar{q}b)_{V-A} \sum_{q'} (\bar{q}' q')_{V+A} \quad \mathcal{Q}_6 = (\bar{q}_i b_j)_{V-A} \sum_{q'} (\bar{q}'_j q'_i)_{V+A} \quad (4)$$

and \mathcal{Q}_7 and \mathcal{Q}_8 are the electromagnetic and chromomagnetic penguin operators:

$$\mathcal{Q}_7 = \frac{e}{8\pi^2} m_b \bar{q} \sigma^{\mu\nu} (1 + \gamma_5) b F_{\mu\nu} \quad \mathcal{Q}_8 = \frac{g}{8\pi^2} m_b \bar{q} \sigma^{\mu\nu} (1 + \gamma_5) T^A b G_{\mu\nu}^A. \quad (5)$$

$q = d$ or s and the convention for the sign of the coupling constants corresponds to the covariant derivative $D_\mu = \partial_\mu + ieQ_f A_\mu + igT^a A_\mu^a$, with A_μ and A_μ^a representing the photon and gluon fields respectively and $Q_e = -1$ etc. The Wilson coefficients C_i are known at next-to-leading order in renormalization group improved perturbation theory [19].

The calculation of the amplitude for $B \rightarrow V\gamma$ decays requires the evaluation of the matrix elements of the weak operators \mathcal{Q}_i listed above. We will restrict our analysis to the phenomenologically relevant operators $\mathcal{Q}_1, \mathcal{Q}_7, \mathcal{Q}_8$: the QCD penguins $\mathcal{Q}_3 \dots \mathcal{Q}_6$ start at $O(\alpha_s)$ and are multiplied by small Wilson coefficients in the weak Hamiltonian \mathcal{H} , whereas the contribution from \mathcal{Q}_2 starts only at $O(\alpha_s^2)$.

The factorisation formula for $B \rightarrow V\gamma$ decays is of the form

$$\frac{G_F}{\sqrt{2}} \lambda_p^{(q)} \langle V\gamma | \mathcal{Q}_i | \bar{B} \rangle = F^{B \rightarrow V}(0) T_i^I + \int \frac{d\tilde{k}_+}{2\pi} du \Phi^B(\tilde{k}_+) T_i^{II}(\tilde{k}_+, u) \Phi_\perp(u), \quad (6)$$

where the non-perturbative effects are contained in $F^{B \rightarrow V}$, a form factor for $B \rightarrow V$ transitions, and Φ^B and Φ_\perp , the leading-twist light-cone distribution amplitudes of the B and V mesons. The hard-scattering amplitudes T_i^I and T_i^{II} include only short-distance effects and are calculable in perturbation theory. The indices p and q have been suppressed on the right-hand side of eq. (6). It is expected that the factorisation formula is valid up to corrections of $O(\Lambda_{\text{QCD}}/m_b)$. Following the analysis in refs. [6, 7], the contribution from the electromagnetic operator \mathcal{Q}_7 is included in the first term on the right-hand side of eq. (6), corresponding to a form factor. The chromomagnetic operator \mathcal{Q}_8 and the four-quark operator \mathcal{Q}_1 contribute to both terms.

The subject of this paper is the second term on the right-hand side of eq. (6), which arises from hard spectator interactions. For such terms factorisation has been explicitly established only at leading order in perturbation theory. We consider the spectator contribution to the matrix element of the chromomagnetic operator \mathcal{Q}_8 , and demonstrate by explicit calculation that the mass singularities at one-loop order are precisely those of the distribution amplitudes in eq. (6). The detailed results for the mass singularities from each diagram are presented in appendix A, together with the terms containing ‘‘large logarithms’’. We analyse the reasons for the factorisation of mass singularities, and present a heuristic demonstration for the matrix elements of \mathcal{Q}_8 in section 3. We then argue that such a cancellation is also valid for the matrix elements of the remaining operators (appendix B), analysing the contribution from \mathcal{Q}_1 , which is expected to be the largest from the four-quark operators $\mathcal{Q}_1 - \mathcal{Q}_6$, in particular detail in section 4. Section 5 contains our conclusions.

1.1 Kinematics

We consider the decay

$$B(p) \rightarrow \gamma(q_1, \varepsilon^*) V(q_2, \eta^*) \quad (7)$$

where p , q_1 and q_2 are the momenta of the corresponding particles and ε^* and η^* are the polarization vectors of the photon and V respectively. We work in the rest frame of the B -meson, $p = (M_B, \vec{0})$, and take the momenta of the photon and V to be in the z -direction, with both final-state vectors transversely polarized.

It is convenient to introduce light-cone coordinates; for any four-vector l we write $l = (l_+, l_-, \vec{l}_\perp)$, with

$$l_\pm = \frac{l_0 \pm l_3}{\sqrt{2}} \quad \text{so that} \quad l^2 = 2l_+l_- - \vec{l}_\perp^2. \quad (8)$$

We neglect the mass of the vector meson, and take q_1 and q_2 to be in the $+$ and $-$ directions respectively:

$$q_1 = \left(\frac{M_B}{\sqrt{2}}, 0, \vec{0}_\perp \right), \quad q_2 = \left(0, \frac{M_B}{\sqrt{2}}, \vec{0}_\perp \right). \quad (9)$$

1.2 Evaluating the T_i^{II}

In this paper we focus on the contribution from the hard spectator interactions represented by the second term on the right-hand side of eq. (6), which we write in the schematic form $\Phi^B \otimes T_i \otimes \Phi_\perp$. Here and in the remainder of the paper, for simplicity of notation, we suppress the superscript II .

In order to verify the validity of the factorisation formula (6) we can use perturbation theory with conveniently chosen partonic external states. In particular we evaluate the hard-scattering kernels T_i , and a signal of the breakdown of factorisation would be the presence of residual long-distance effects in the T_i . For our calculations we take the initial state to have momentum p and to consist of a b -quark with momentum $p-k$ and a light (spectator) antiquark \bar{q}' with momentum k . The components of k are of $O(\Lambda_{\text{QCD}})$. Our final state consists of the photon with momentum q_1 and a quark (q) and spectator antiquark (\bar{q}') with momenta $\bar{x}q_2$ and xq_2 respectively. The partons in the initial and final states are on their mass shells. The hard-scattering kernel is obtained in the standard way; by using perturbation theory to calculate the matrix elements of the operator \mathcal{Q}_i between these states together with the light-cone distribution amplitudes (defined explicitly in the next subsection) for the initial and final partonic states. Let \mathcal{A}_i denote the left hand side of eq. (6) and the superscript (n) label the perturbative contributions of $O(\alpha_s^n)$ relative to the lowest order (denoted by (0)). The hard-scattering kernels at one-loop order ($T_i^{(1)}$) are then obtained by rewriting the factorisation formula as

$$\Phi^{b\bar{q}'(0)} \otimes T_i^{(1)} \otimes \Phi^{q\bar{q}'(0)} = \mathcal{A}_i^{(1)} - \Phi^{b\bar{q}'(1)} \otimes T_i^{(0)} \otimes \Phi^{q\bar{q}'(0)} - \Phi^{b\bar{q}'(0)} \otimes T_i^{(0)} \otimes \Phi^{q\bar{q}'(1)}, \quad (10)$$

where the Φ 's denote the corresponding distribution amplitudes. We confirm below that although there are mass singularities in the $\mathcal{A}_i^{(1)}$, they are cancelled by the remaining terms on the right-hand side of eq. (10).

Throughout this paper the discussion of the contributions from particular diagrams corresponds to the Feynman gauge.

1.3 Light-Cone Distribution Amplitudes

We define the light-cone distribution amplitude of a state H containing the b -quark by

$$\Phi_{\alpha\beta}^H(\tilde{k}_+) = \int dz_- e^{i\tilde{k}_+ z_-} \langle 0 | \bar{q}'_{\beta}(z) [z, 0] b_{\alpha}(0) | H \rangle |_{z_+, z_{\perp}=0}, \quad (11)$$

where q', b are the quark fields and α, β are spinor labels (we denote the spectator antiquark by \bar{q}'). $[z, 0]$ denotes the path-ordered exponential, $\mathcal{P} \exp[-ig \int_0^z dx^{\mu} A_{\mu}(x)]$. Ultimately of course, when evaluating the physical decay amplitude we use the distribution amplitude of the B -meson, but in the evaluation of the hard-scattering amplitude T_i in perturbation theory we take H to be a quark-antiquark state.

Similarly the light-cone distribution amplitude of a light state L is defined by:

$$\Phi_{\gamma\delta}^L(u) = q_{2-} \int \frac{d(y-x)_+}{2\pi} e^{-i(uq_2 \cdot x + \bar{u}q_2 \cdot y)} \langle L | \bar{q}_{\delta}(y) [y, x] q'_{\gamma}(x) | 0 \rangle |_{(x-y)_-, (x-y)_{\perp}=0}, \quad (12)$$

where $\bar{u} = 1 - u$, and the integrand in eq. (12) is a function of $(x-y)_+$.

In terms of the definitions in equations (11) and (12), for the B and V mesons we follow an equivalent spinor decomposition to that in refs. [20, 5, 6] and define the distribution amplitudes $\Phi_{\pm}^B(\tilde{k}_+)$ and $\Phi_{\perp}(u)$ by ²

$$\Phi_{\alpha\beta}^B(\tilde{k}_+) = -\frac{if_B M_B}{4} \left\{ (1 + \not{v}) \left[\Phi_{+}^B(\tilde{k}_+) + \not{n}_- (\Phi_{-}^B(\tilde{k}_+) - \Phi_{+}^B(\tilde{k}_+)) \right] \gamma_5 \right\}_{\alpha\beta} \quad (13)$$

$$\Phi_{\gamma\delta}^V(u) = -\frac{if_V^{\perp}}{4} (\sigma_{\mu\nu})_{\gamma\delta} (\eta^*)^{\mu} q_2^{\nu} \Phi_{\perp}(u) = \frac{f_V^{\perp}}{4} \not{\eta}^* \not{q}_2 \Phi_{\perp}(u), \quad (14)$$

where the light-like vector n_- is given in light-cone coordinates by $n_- = (0, \sqrt{2}, \vec{0}_{\perp})$, and the four velocity v is defined by $p_{\mu} = M_B v_{\mu}$. The decay constants f_B and f_V^{\perp} are defined by

$$\langle 0 | \bar{q}'_{\gamma} \gamma_{\mu} \gamma_5 b | \bar{B}(p) \rangle = if_B p_{\mu} \quad \text{and} \quad \langle V(k, \eta^*) | \bar{q} \sigma_{\mu\nu} q' | 0 \rangle = -i(\eta_{\mu}^* k_{\nu} - \eta_{\nu}^* k_{\mu}) f_V^{\perp}. \quad (15)$$

2 Leading Order Results for the Matrix Elements of the Operators \mathcal{Q}_8 and \mathcal{Q}_1

Before studying the cancellation of mass singularities at next-to-leading order (NLO) in perturbation theory, we present the lowest-order contributions to the hard-scattering amplitude from the operators \mathcal{Q}_8 and \mathcal{Q}_1 respectively.

2.1 Tree-Level Result for the matrix element of \mathcal{Q}_8

As explained above, we determine the hard-scattering amplitude T_8 by choosing the convenient external states $H = b\bar{q}'$ and $L = q\bar{q}'$ and computing both the matrix element

$$\mathcal{A}_8 \equiv -\frac{G_F \lambda_t^{(q)}}{\sqrt{2}} \langle L \gamma | \mathcal{Q}_8 | H \rangle \quad (16)$$

²Following ref. [11, 12], Φ_{\pm}^B is defined in the Heavy-Quark Effective Theory, but with the physical decay constant f_B in front of it. It was pointed out in ref. [21] that a different normalisation factor can be chosen to ensure a more natural comparison with HQET results. Such a change in the normalisation of Φ_{\pm}^B does not affect the outcome of our analysis and corresponds to a simple redistribution of terms between the hard-scattering kernel T^{II} and the B -meson's light-cone distribution amplitude.

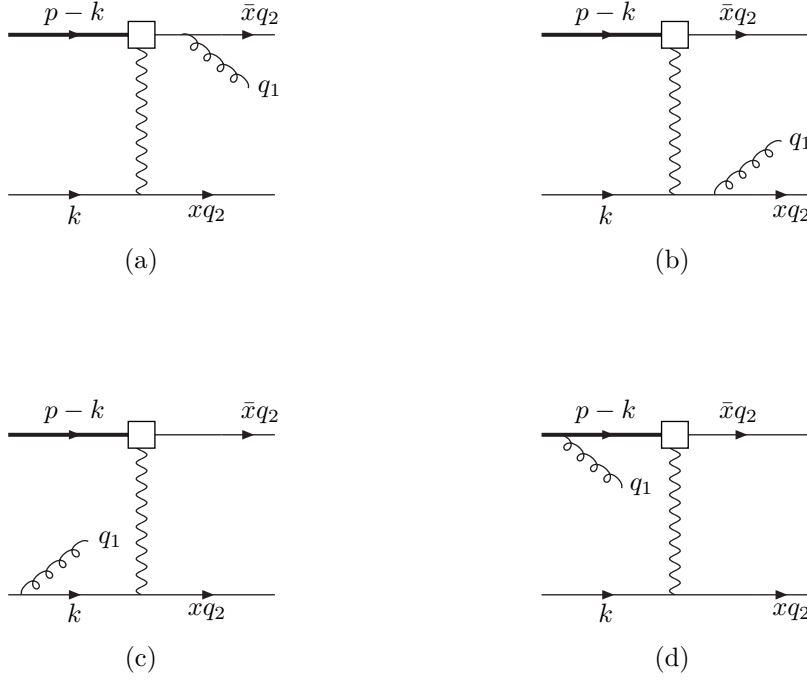


Figure 1: Lowest-order contributions to the matrix element $\langle \bar{q}'(xq_2) q(\bar{x}q_2) \gamma(q_1) | \mathcal{Q}_8 | \bar{q}'(k) b(p-k) \rangle$. The spring-like line represents the photon and the square denotes the insertion of \mathcal{Q}_8 .

and the distribution amplitudes $\Phi^{H,L}$. In this section the calculation is performed at lowest order of perturbation theory.

There are four diagrams contributing to \mathcal{A}_8 at lowest order, and these are shown in fig. 1. At leading twist only the diagram of fig. 1(a) contributes and we find:

$$\mathcal{A}_8^{(0)} = -G_F \lambda_t^{(q)} \frac{eQ_q \alpha_s}{2\pi} \frac{1}{\bar{x}\tilde{k}_+} \left(\bar{u}(\bar{x}q_2) \{ \not{\epsilon}^* \gamma_\nu (1 + \gamma_5) T^A \} u(p-k) \right) \left(\bar{v}(k) \{ \gamma^\nu T^A \} v(xq_2) \right), \quad (17)$$

where u and v represent the free-particle spinor wave functions and $Q_q = -1/3$ is the charge of the quark q .

The distribution amplitudes at lowest order are:

$$\Phi_{\alpha\beta}^{b\bar{q}'}^{(0)}(\tilde{k}_+) = 2\pi \delta(k_+ - \tilde{k}_+) \bar{v}_\beta(k) u_\alpha(p-k) \quad (18)$$

$$\Phi_{\gamma\delta}^{q\bar{q}'}^{(0)}(u) = \delta(u-x) \bar{u}_\delta(\bar{x}q_2) v_\gamma(xq_2), \quad (19)$$

and $\mathcal{A}_8^{(0)}$ can be written in the factorised form

$$\mathcal{A}_8^{(0)} = \Phi^{b\bar{q}'}^{(0)} \otimes T_8^{(0)} \otimes \Phi^{q\bar{q}'}^{(0)} \quad (20)$$

with

$$T_8^{(0)}{}_{\alpha\beta\gamma\delta}(\tilde{k}_+, u) = -G_F \lambda_t^{(q)} \frac{eQ_q \alpha_s}{2\pi} \frac{1}{\bar{u}\tilde{k}_+} \{ \not{\epsilon}^* \gamma_\nu (1 + \gamma_5) T^A \}_{\delta\alpha} \{ \gamma^\nu T^A \}_{\beta\gamma}. \quad (21)$$

For simplicity of notation, we have suppressed the colour indices. $T_8^{(0)}$ is a function of the convolution variables \tilde{k}_+ and u , but does not depend on any kinematical quantities of $O(\Lambda_{\text{QCD}})$.



Figure 2: Lowest-order contribution to the matrix element $\langle \bar{q}'(xq_2) q(\bar{x}q_2) | \mathcal{Q}_1 | \bar{q}'(k) b(p-k) \rangle$. The arrow on the quark loop defines the direction of the flow of fermion number.

We conclude the lowest-order calculation by briefly considering the three diagrams in fig. 1(b)–(d). Fig. 1(b) manifestly gives a higher-twist contribution, since both the gluon and internal antiquark are off-shell by an amount of $O(M_B^2)$. In diagram 1(c), although the gluon is off-shell by $O(M_B^2)$, the internal antiquark is off-shell by $O((q_1 - k)^2) = O(M_B \Lambda_{\text{QCD}})$. However this potentially leading-twist contribution vanishes when projected with the wave function of a transversely polarized vector meson (see eq. (14)). The contribution from diagram 1(d) vanishes by the equations of motion of the final-state meson.

2.2 Lowest-order result for the matrix element of \mathcal{Q}_1

The second example which we study in some detail is the matrix element of the operator \mathcal{Q}_1 . At lowest order the relevant diagrams are shown in fig. 2. The contribution proportional to $\lambda_c^{(q)}$ ($\lambda_u^{(q)}$) is the difference of the diagrams with the charm (up) quark propagating in the loop and one with the top quark. Here we present the results for the charm quark (the corresponding results for the up quark can readily be deduced from these):

$$\mathcal{A}_1 \equiv \frac{G_F \lambda_c^{(q)}}{\sqrt{2}} \langle L \gamma | (\bar{q}c)_{V-A} (\bar{c}b)_{V-A} | H \rangle. \quad (22)$$

Following ref. [6], we do not neglect m_c^2/m_b^2 , and hence keep an important imaginary part which vanishes when m_c is set to zero.

Evaluating the diagrams in fig. 2 we find:

$$\begin{aligned} \mathcal{A}_1^{(0)} &= i \frac{G_F \lambda_c^{(q)}}{\sqrt{2}} \frac{e Q_c \alpha_s}{4\pi} \frac{2}{xq_2 - k_+} \left(\bar{u}(\bar{x}q_2) \gamma_\nu (1 - \gamma_5) T^a u(p-k) \right) \left(\bar{v}(k) \gamma_\rho T^a v(xq_2) \right) \times \\ &\left\{ T_1(x, s) \epsilon^{\sigma\rho\lambda\nu} (xq_2 - q_1)_\sigma + T_2(x, s) \epsilon^{\sigma\lambda\tau\nu} q_1^\rho q_{1\sigma} q_{2\tau} + T_3(x, s) \epsilon^{\sigma\rho\tau\lambda} q_1^\nu q_{1\sigma} q_{2\tau} \right\} \times \varepsilon_\lambda^*, \end{aligned} \quad (23)$$

where $Q_c = 2/3$ is the charge of the charm quark, $s = m_c^2/m_b^2$,

$$T_1(x, s) = -\frac{1}{3} + \frac{4s}{x} - \frac{2s}{x} L, \quad (24)$$

$$T_2(x, s) = \frac{1}{M_B^2} \left(\frac{2}{3} - \frac{8s}{x} + \frac{4s}{x} L \right), \quad (25)$$

$$T_3(x, s) = -\frac{1}{M_B^2} \left(\frac{4}{3} + \frac{8s}{x} - \frac{4s}{x} (L + P) \right), \quad (26)$$

with

$$L = \sqrt{1 - 4s/x + i\epsilon} \log \left(\frac{\sqrt{1 - 4s/x + i\epsilon} + 1}{\sqrt{1 - 4s/x + i\epsilon} - 1} \right) \quad (27)$$

and

$$P = L_2 \left(\frac{2}{1 - \sqrt{\frac{x-4s+i\epsilon}{x}}} \right) + L_2 \left(\frac{2}{1 + \sqrt{\frac{x-4s+i\epsilon}{x}}} \right), \quad (28)$$

where L_2 is the dilogarithm function. From eq. (23) and the tree-level expressions for the distribution amplitudes in equations (18) and (19) one immediately obtains the lowest-order contribution to the hard-scattering kernel $T_1^{(0)}$.

2.3 Predictions for the Spectator Contributions to $B \rightarrow V\gamma$ Decay Amplitudes at Lowest Order

In order to obtain the predictions for the spectator contributions to $B \rightarrow V\gamma$ decay amplitudes, the hard-scattering kernels obtained in the previous two subsections need to be convoluted with the B and V distribution amplitudes. Convoluting the lowest-order result for the hard-scattering kernel $T_8^{(0)}$ in eq. (21) with the distribution amplitudes we obtain for the spectator contribution to the amplitude

$$\begin{aligned} -\frac{G_F \lambda_t^{(q)}}{\sqrt{2}} \langle V\gamma | \mathcal{Q}_8 | \bar{B} \rangle &= -(G_F \lambda_t^{(q)}) \frac{\alpha_s C_F}{4\pi} \frac{f_B f_V^\perp}{N} (eQ_q) \int \frac{d\tilde{k}_+}{2\pi} \frac{\Phi_+^B(\tilde{k}_+)}{\tilde{k}_+} \int du \frac{\Phi_V^\perp(u)}{\bar{u}} \\ &\times \left\{ \varepsilon_{\mu\nu\lambda\rho} \varepsilon^{*\mu} \eta^{*\nu} q_2^\lambda q_1^\rho + i(\varepsilon^* \cdot \eta^*)(q_1 \cdot q_2) \right\}, \end{aligned} \quad (29)$$

where $Q_q = -1/3$ is the charge of the down or strange quark and $N = 3$ is the number of colours. This is equivalent to the result in eqs. (39) and (40) of ref. [6].

Similarly, convoluting the hard-scattering kernel $T_1^{(0)}$ from the lowest-order amplitude in eq. (23) with the B and V -meson distribution amplitudes we obtain

$$\begin{aligned} \frac{G_F \lambda_c^{(q)}}{\sqrt{2}} \langle V\gamma | \mathcal{Q}_1^c | \bar{B} \rangle &= \frac{G_F \lambda_c^{(q)}}{4} \frac{\alpha_s C_F}{4\pi} \frac{f_B f_V^\perp}{N} (eQ_u) \int \frac{d\tilde{k}_+}{2\pi} \frac{\Phi_+^B(\tilde{k}_+)}{\tilde{k}_+} \int du \Phi_V^\perp(u) h(u, s) \\ &\times \left\{ \varepsilon_{\mu\nu\lambda\rho} \varepsilon^{*\mu} \eta^{*\nu} q_2^\lambda q_1^\rho + i(\varepsilon^* \cdot \eta^*)(q_1 \cdot q_2) \right\}, \end{aligned} \quad (30)$$

where

$$h(u, s) = -\frac{2}{u} + \frac{4s}{u^2} \left\{ L_2 \left(\frac{2}{1 - \sqrt{\frac{u-4s+i\epsilon}{u}}} \right) + L_2 \left(\frac{2}{1 + \sqrt{\frac{u-4s+i\epsilon}{u}}} \right) \right\}. \quad (31)$$

If m_c is set to zero, $h(u, 0) = -2/u$. These results are equivalent to those in eqs. (33)–(35) of ref. [6].

3 Factorisation at One-Loop Order for the Chromomagnetic Operator \mathcal{Q}_8

We now turn to the main subject of this paper, the factorisation of mass singularities at one-loop order for the spectator interactions. We start with the operator \mathcal{Q}_8 and study the one-loop corrections to the lowest-order diagram in fig. 1(a). We redraw this diagram in fig. 3, labelling the external lines by (1)–(4), the internal propagators by (5) and (6) and the weak vertex by

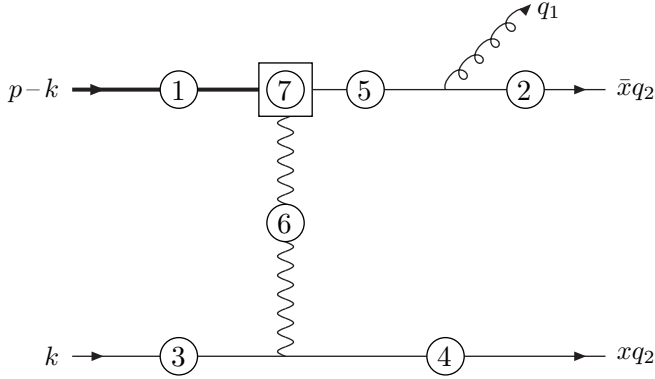


Figure 3: Notation for one-loop diagrams contributing to the $B \rightarrow V\gamma$ decay from \mathcal{Q}_8 . The extra gluon can be attached to any pair of circles (which might be identical).

(7). The mass singularities at NLO arise from diagrams in which a gluon is attached to two of the circles in fig. 3 (including diagrams in which both ends of the gluon are attached to the same circle). We denote by (ij) the diagram obtained by adding a gluon between the circles (i) and (j) (see, for example, fig. 4 where diagrams (34), (23) and (13) are drawn explicitly). We evaluate the terms containing the mass singularities and/or large logarithms which are of the form $\log(M_B^2/q_2 \cdot k)$.

We present the results from an explicit evaluation of each diagram in Appendix A, from which the cancellation of mass singularities from the hard-scattering kernel is apparent. In the calculation presented in the appendix we do not make any a priori assumptions about the regions of phase space which lead to mass singularities or large logarithms. In this section we demonstrate the cancellation of mass singularities using a heuristic argument, based on power counting, which shows that the mass singularities arise from regions in which the gluon is soft or collinear with q_2 or k (including contributions from the *soft-collinear* region of phase-space [24]). In Appendix B we argue further that such a cancellation holds for all the weak operators in the effective Hamiltonian of eq. (1).

We emphasize that not all the one-loop corrections are given by the set of diagrams $\{(ij)\}$, and for illustration in figure 9 we draw an additional Feynman diagram (called D). However, all the mass singularities are given by diagrams (ij) and only these diagrams and diagram D give large logarithms. The remaining diagrams, which may contribute either to T^I or T^{II} , are only sensitive to physics at scales of $O(M_B)$.

We implement a similar notation for diagrams which give the one-loop corrections to the distribution amplitudes, and which therefore contribute to $\Phi^{b\bar{q}'(1)} \otimes T^{(0)} \otimes \Phi^{q\bar{q}'(0)}$ and $\Phi^{b\bar{q}'(0)} \otimes T^{(0)} \otimes \Phi^{q\bar{q}'(1)}$ (see eq. (10)). By $(13)'$, $(11)'$ and $(33)'$ we denote the contribution to $\Phi^{b\bar{q}'(1)} \otimes T^{(0)} \otimes \Phi^{q\bar{q}'(0)}$ in which the gluon in the one-loop correction to the distribution amplitude of the initial $b\bar{q}'$ state ($\Phi^{b\bar{q}'(1)}$) is attached to lines 1 and 3 as indicated (where 1 denotes the b -quark and 3 the spectator antiquark). Similarly by $(24)'$, $(22)'$ and $(44)'$ we denote the contribution to $\Phi^{b\bar{q}'(0)} \otimes T^{(0)} \otimes \Phi^{q\bar{q}'(1)}$ in which the gluon in the one-loop correction to the distribution amplitude of the final $q\bar{q}'$ state ($\Phi^{q\bar{q}'(1)}$) is attached to lines 2 and 4 as indicated (where 2 and 4 denote the quark and spectator antiquark respectively). There are also corrections to the distribution amplitudes in which one end of the gluon is attached to the path-ordered exponential. By $(1B)'$

$((3B)')$ we denote the contribution to $\Phi^{b\bar{q}'(1)} \otimes T^{(0)} \otimes \Phi^{q\bar{q}'(0)}$ in which one end of the gluon in the one-loop correction to the distribution amplitude of the initial $b\bar{q}'$ state is attached to line 1 (line 3) and the other to the path-ordered exponential. Similarly by $(2V)'$ ($(4V)'$) we denote the contribution to $\Phi^{b\bar{q}'(0)} \otimes T^{(0)} \otimes \Phi^{q\bar{q}'(1)}$ in which one end of the gluon in the one-loop correction to the distribution amplitude of the final $q\bar{q}'$ state is attached to line 2 (line 4) and the other to the path-ordered exponential.

We now present our heuristic diagrammatic argument for the cancellation of the mass singularities. In Appendix B we give a formal argument explaining the reasons for this cancellation based on the collinear Ward identity.

3.1 Cancellation of Soft Divergences

We start by considering soft divergences, which arise when the loop momentum is small, with all components vanishing in a similar way. Such divergences arise in diagrams with a gluon attached to two external lines. As explained below, some of these divergences are absorbed into the mesons' distribution amplitudes in a straightforward manner. The cancellation of the remaining infrared divergences occurs as expected from arguments based on *colour transparency* [22]. Soft gluons only couple to the compact, colour-singlet vector state through a dipole interaction, which is non-singular. In terms of Feynman diagrams there is a cancellation of infrared divergences between graphs in which the soft gluons couple to different constituents of the vector meson.

To illustrate this point consider the graph (34), drawn explicitly in fig. 4, which is singular in the soft region, $l^\mu \rightarrow 0$. The contribution from this region is

$$\begin{aligned}
(34) &= -ig^2 \left(C_F - \frac{C_A}{2} \right) \mathcal{A}_8^{(0)} \int \frac{d^4 l}{(2\pi)^4} \frac{4(k-l) \cdot xq_2}{l^2(l-k)^2(xq_2-l)^2} \\
&\simeq 2ig^2 \left(C_F - \frac{C_A}{2} \right) \mathcal{A}_8^{(0)} \int \frac{d^4 l}{(2\pi)^4} \frac{(k-l) \cdot q_2}{l^2(l-k)^2(q_2 \cdot l)}. \tag{32}
\end{aligned}$$

In the soft region the contribution from diagram (23) (also drawn in fig. 4) is

$$\begin{aligned}
(23) &= ig^2 \left(C_F - \frac{C_A}{2} \right) \mathcal{A}_8^{(0)} \int \frac{d^4 l}{(2\pi)^4} \frac{4(k-l) \cdot \bar{x}q_2}{l^2(l-k)^2(\bar{x}q_2-l)^2} \\
&\simeq -2ig^2 \left(C_F - \frac{C_A}{2} \right) \mathcal{A}_8^{(0)} \int \frac{d^4 l}{(2\pi)^4} \frac{(k-l) \cdot q_2}{l^2(l-k)^2(q_2 \cdot l)} = -(34). \tag{33}
\end{aligned}$$

The soft divergences in diagrams (12) and (14) cancel in an analogous way. In addition there are soft divergences in the self-energy diagrams (nn) ($n=1-4$), but these are trivially absorbed into the B and vector-meson light-cone wave functions (diagrams $(nn)'$, with $n=1-4$).

Before proceeding to a discussion of collinear divergences, we briefly comment on diagram (13) drawn in fig. 4. By power counting one can readily demonstrate that this diagram has a leading-twist contribution from the soft region in which the components of l are $O(\Lambda_{\text{QCD}})$. This contribution is also absorbed into the corresponding distribution amplitude; specifically the contribution from diagram (13) is cancelled by the subtraction of the corresponding term in $\Phi^{b\bar{q}'(1)} \otimes T^{(0)} \otimes \Phi^{q\bar{q}'(0)}$ (i.e. by the subtraction of diagram (13)' in which the diagram contributing to $\Phi^{b\bar{q}'(1)}$ is also drawn in fig. 4). The reason for such cancellations has been explained in detail in ref. [11]. Diagram (13)' differs from (13) in that the propagator of the gluon attached to the weak vertex is replaced by its eikonal approximation $((xq_2 - k + l)^2 \rightarrow -2xq_2 \cdot (k - l))$.

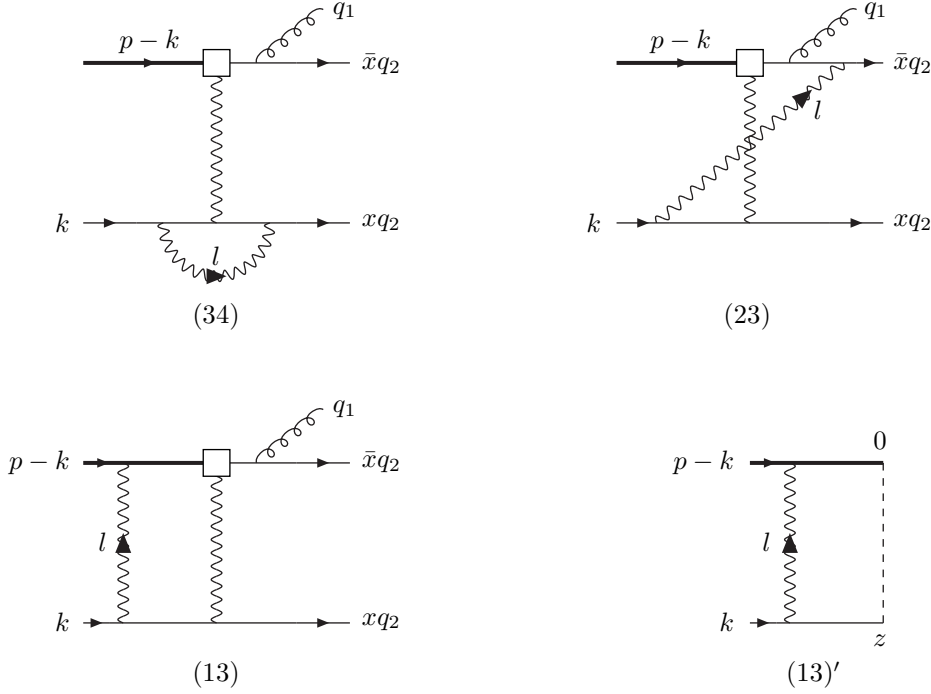


Figure 4: The one-loop graphs (34), (23) and (13) contributing to the decay amplitude and a diagram which contributes to the distribution amplitude of the initial state $\Phi^{b\bar{q}'}(1)$. The dashed line represents the path-ordered exponential and $z^2 = 0$.

Since the leading-twist contribution in (13) comes from the soft region, we can approximate this propagator by the eikonal form in this diagram. Thus the two contributions are equal and therefore cancel in the evaluation of the hard-scattering amplitude. Diagrams (24) and (24)' do not have such leading-twist contributions from the soft region.

3.2 Cancellation of Collinear Divergences

We now consider collinear divergences, present when a gluon is attached to an external light-quark line. Such singularities can occur when the gluon is parallel to the momentum of the vector meson q_2 or to the momentum of the spectator antiquark k (in this latter case, since $k = O(\Lambda_{\text{QCD}})$, one does not call the corresponding gluons *collinear* in the standard SCET nomenclature). We distinguish between these two cases, beginning our discussion with the former.

3.2.1 Divergences from the Region Collinear to q_2

In this section we consider the region of phase space in which the loop momentum is parallel to q_2 . There are corresponding mass singularities in diagrams with a gluon attached to one of the final-state external lines, 2 or 4. Before evaluating each diagram in turn, it is convenient to consider the distribution amplitude of the final state, in this case the state with a light quark and a light anti-quark with momenta $\bar{x}q_2$ and xq_2 respectively:

$$\Phi_{\alpha\beta}^{q\bar{q}'}(u) = q_{2-} \int \frac{dz_+}{2\pi} e^{-i(uq_2 \cdot x + \bar{u}q_2 \cdot y)} \langle \bar{q}'(xq_2) q(\bar{x}q_2) | \bar{q}'_{\beta}(y)[y, x] q_{\alpha}(x) | 0 \rangle, \quad (34)$$

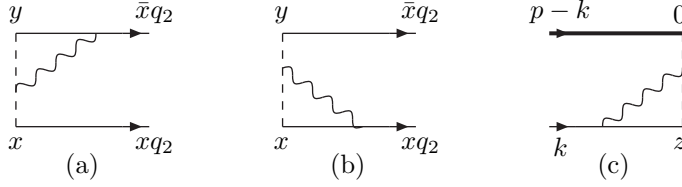


Figure 5: Two one-loop diagrams contributing to the distribution amplitude of the $q\bar{q}'$ final state, (a) and (b), and a diagram contributing to the distribution amplitude of the $b\bar{q}'$ final state. The dashed line represents the path-ordered exponential and $z^2 = (x - y)^2 = 0$.

where $z = x - y$, α and β are spinor labels and $[y, x]$ represents the path-ordered exponential between the two points y and x .

We have seen above that for the free theory (see eq. (19))

$$\Phi_{\alpha\beta}^{q\bar{q}'}{}^{(0)}(u) = \delta(u - x) \bar{u}_\beta(\bar{x}q_2) v_\alpha(xq_2), \quad (35)$$

where \bar{u}_β and v_α are free Dirac spinors. Now consider the contributions to the distribution amplitude from the two one-loop diagrams in fig. 5(a) and (b), in which a gluon is attached at one end to the path-ordered exponential³. In the collinear region in which l , the momentum of the gluon, is parallel to q_2 ($l \simeq \xi q_2$, with the remaining components of l vanishing as $l_+ \sim \lambda^2/l_-$ and $l_\perp \sim \lambda$ as $\lambda \rightarrow 0$) their contributions can be written as:

$$\begin{aligned} \Phi_{(a)\alpha\beta}^{q\bar{q}'}{}^{(1)}(u) &= \bar{u}_\beta(\bar{x}q_2) v_\alpha(xq_2) \times \\ & (2ig^2 C_F) \int \frac{d^4l}{(2\pi)^4} \frac{\bar{x} - \xi}{\xi} \frac{1}{l^2} \frac{1}{(\bar{x}q_2 - l)^2} \{ \delta(u - x) - \delta(u - x - \xi) \}, \end{aligned} \quad (36)$$

$$\begin{aligned} \Phi_{(b)\alpha\beta}^{q\bar{q}'}{}^{(1)}(u) &= \bar{u}_\beta(\bar{x}q_2) v_\alpha(xq_2) \times \\ & (2ig^2 C_F) \int \frac{d^4l}{(2\pi)^4} \frac{x - \xi}{\xi} \frac{1}{l^2} \frac{1}{(xq_2 - l)^2} \{ \delta(u - x) - \delta(u - x + \xi) \}, \end{aligned} \quad (37)$$

where the subscripts (a) and (b) refer to the corresponding diagrams in fig. 5. We will use the representations in eqs. (36) and (37) in our discussion below. For the other diagrams contributing to the wave function of the final state at one-loop order it will be very straightforward to see how the mass singularities are precisely those needed to absorb the corresponding ones from the amplitude.

In order to illustrate the cancellation of collinear divergences coming from the region of phase space in which the momentum of gluon(s) in the loop is(are) parallel to q_2 consider diagram (12). Since we are considering the collinear divergence we set $l \simeq \xi q_2$, with ξ finite and the remaining components of l vanish as $l_+ \sim \lambda^2/l_-$ and $l_\perp \sim \lambda$ in the singular region $\lambda \rightarrow 0$. Keeping only the leading-twist terms one readily finds

$$(12) = 2ig^2 \left(C_F - \frac{C_A}{2} \right) \mathcal{A}_8^{(0)} \int \frac{d^4l}{(2\pi)^4} \frac{\bar{x}}{\xi} \frac{1}{l^2} \frac{1}{(\bar{x}q_2 - l)^2}. \quad (38)$$

The integral over l_+ and l_\perp gives a collinear divergence. These collinear divergences also cancel, but in a different way to the soft divergences. In this case it is straightforward to verify that in the region where l is collinear to q_2 ,

$$(23) = -(12), \quad (39)$$

³The remaining one-loop diagrams contributing to the distribution amplitude will be discussed later.

so that the corresponding collinear divergences cancel between diagrams (12) and (23). As we will see when we consider the cancellation of collinear divergences for the operator \mathcal{Q}_1 below, such a cancellation between pairs of diagrams is not typical. What is required however, is that apart from the propagators which are explicitly exhibited in eq. (38) ($1/l^2$ and $1/(\bar{x}q_2 - l)^2$) one can replace l by ξq_2 everywhere.

There are similar cancellations between other pairs of diagrams ⁴

$$(14) = -(34) = -2ig^2 \left(C_F - \frac{C_A}{2} \right) \mathcal{A}_8^{(0)} \int \frac{d^4l}{(2\pi)^4} \frac{x - \xi}{\xi} \frac{1}{l^2} \frac{1}{(xq_2 - l)^2}; \quad (40)$$

$$(26) = -(27) = ig^2 C_A \mathcal{A}_8^{(0)} \frac{\bar{x}}{x} \int \frac{d^4l}{(2\pi)^4} \frac{1}{l^2} \frac{1}{(\bar{x}q_2 - l)^2}; \quad (41)$$

$$(36) = -(37) = -ig^2 C_A \mathcal{A}_8^{(0)} \int \frac{d^4l}{(2\pi)^4} \frac{1}{l^2} \frac{1}{(xq_2 - l)^2}. \quad (42)$$

This leaves us with the collinear divergences from diagrams (25) and (45) in which one end of the additional gluon is attached to the internal quark propagator 5. These are precisely the terms which are absorbed into the wave function of the final state (in this case the $q\bar{q}'$ state), i.e. the divergences in the contributions from diagrams (25) and (45) to $\mathcal{A}_8^{(1)}$ are cancelled by the subtraction of $\Phi^{b\bar{q}'}(0) \otimes T_8^{(0)} \otimes \Phi^{q\bar{q}'}(1)$ in eq. (10). More specifically they are cancelled by the contributions to the wave function from the diagrams in fig. 5(a) and (b), which we denote by $(2V)'$ and $(4V)'$ respectively. Using the expressions in eqs. (36) and (37), it is straightforward to demonstrate that in this collinear region

$$(25) = (2V)' = -2ig^2 C_F \mathcal{A}_8^{(0)} \int \frac{d^4l}{(2\pi)^4} \frac{1}{l^2} \frac{1}{(\bar{x}q_2 - l)^2}; \quad (43)$$

$$(45) = (4V)' = 2ig^2 C_F \mathcal{A}_8^{(0)} \int \frac{d^4l}{(2\pi)^4} \frac{x - \xi}{\bar{x} + \xi} \frac{1}{l^2} \frac{1}{(xq_2 - l)^2}. \quad (44)$$

Finally we discuss the contribution of diagram (24). For the processes considered in this paper, with a transversely polarized vector meson in the final state, the leading-twist contribution vanishes. We therefore do not discuss this further, other than to note that for a generic final state this contribution is cancelled by the corresponding one in $\Phi^{b\bar{q}'}(0) \otimes T_8^{(0)} \otimes \Phi^{q\bar{q}'}(1)$.

Thus we find that, at one-loop order, there are no singular contributions to $T_8^{(1)}$ from the region in which the momentum of the gluon l is parallel to q_2 , and that the cancellation of the singularities has a very simple structure. The divergences either cancel between pairs of diagrams contributing to $\mathcal{A}_8^{(1)}$, or between diagrams contributing to $\mathcal{A}_8^{(1)}$ and to $\Phi^{b\bar{q}'}(0) \otimes T_8^{(0)} \otimes \Phi^{q\bar{q}'}(1)$.

3.2.2 Divergences from the Region Collinear to k

For the B -meson initial state, the momentum of the spectator antiquark, k , is generically soft, with all components of $O(\Lambda_{\text{QCD}})$. In our calculations we take k to be light-like so that long-distance effects are manifested by the presence of mass singularities, specifically collinear divergences from the region of phase space where the momenta of internal partons are collinear with

⁴The mass singularities considered in this section appear in diagrams in which a gluon in a loop is attached to one of the final-state external lines 2 or 4. Below however, we give singular expressions for diagrams (36) and (37). These diagrams could equally well have been denoted by (46) and (47) and hence are indeed singular.

k (as well as the soft divergences discussed above). We now consider these collinear divergences. The diagrams which can have such a divergence contain a gluon line attached to the external line 3. Writing $l \simeq \sigma k$ with l_- and l_\perp vanishing with λ as λ^2/l_+ and λ respectively, we readily find the following three leading-twist contributions (diagram (37)=0 and (35) gives a higher-twist contribution):

$$(23) = -2ig^2 \left(C_F - \frac{C_A}{2} \right) \mathcal{A}_8^{(0)} \int \frac{d^4l}{(2\pi)^4} \frac{1}{\sigma} \frac{1}{l^2 (k-l)^2}, \quad (45)$$

$$(34) = 2ig^2 \left(C_F - \frac{C_A}{2} \right) \mathcal{A}_8^{(0)} \int \frac{d^4l}{(2\pi)^4} \frac{1-\sigma}{\sigma} \frac{1}{l^2 (k-l)^2}, \quad (46)$$

$$(36) = -ig^2 C_A \mathcal{A}_8^{(0)} \int \frac{d^4l}{(2\pi)^4} \frac{1}{l^2 (k-l)^2}. \quad (47)$$

Summing these contributions we obtain

$$(23) + (34) + (36) = -2ig^2 C_F \mathcal{A}_8^{(0)} \int \frac{d^4l}{(2\pi)^4} \frac{1}{l^2 (k-l)^2} = (3B)', \quad (48)$$

where $(3B)'$ is the corresponding one-loop contribution to $\Phi^{b\bar{q}'}^{(1)} \otimes T_8^{(0)} \otimes \Phi^{q\bar{q}'}^{(0)}$, i.e. the one from the contribution of the graph in fig. 5(c) to $\Phi^{b\bar{q}'}^{(1)}$. Thus there are no collinear singularities in $T_8^{(1)}$ arising from the region in which l is parallel to k .

3.3 Double Logarithms

In sections 3.1 and 3.2 we have analyzed the regions of phase space in which the momentum of a gluon in the loop was either soft or collinear with q_2 or k , and deduced that the cancellation of the corresponding divergences is straightforward. We now briefly analyze the region in which the gluons are both soft and collinear, which leads to double logarithms in an infrared cut-off for some of the diagrams.

The double logarithms arise in diagrams (12) and (14) as $\xi \rightarrow 0$ (see equations (38) and (40)) and in diagrams (23) and (34) as either $\xi \rightarrow 0$ (equations (38), (39) and (40)) or $\sigma \rightarrow 0$ (equations (45) and (46)). Explicit evaluation of the diagrams, described in Appendix A, confirms that only these four diagrams contain double logarithms.

From the expressions in the previous subsections we can also deduce how the double logarithms cancel. We know from section 3.1 that the soft divergences cancel in the sum of diagrams (23)+(34), and from equations (45) and (46) we note that the term which diverges as $1/\sigma$ as $\sigma \rightarrow 0$ cancels in the integrand of (23)+(34). Thus the double logarithms in diagrams (23) and (34) cancel, leaving only a collinear divergence from the region in which l is parallel to q_2 . This is confirmed by explicit calculations (see eqs. (79) and (80) in Appendix A). Similarly, since the soft divergences cancel in diagrams (12) and (14), in the sum of these two diagrams we are only left with a single logarithm corresponding to a collinear divergence from the region in which l is parallel to q_2 .

When presenting such heuristic arguments, one has to consider the possibility that, after the cancellation of the double logarithms, a subtlety in the way that the integrals are regulated may leave a single logarithm which had not been considered. The explicit calculations in appendix A clearly remove such worries, but it is also relatively straightforward to verify this without the full computations. For example one may evaluate either the l_- or l_+ integration by contours, and readily verify the above pattern of cancellations.

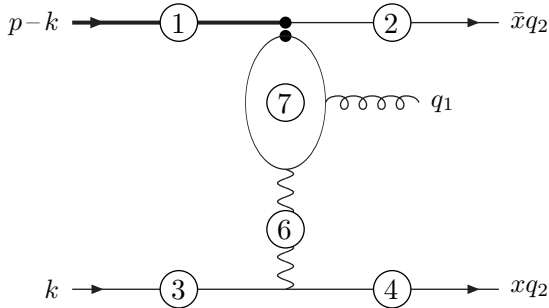


Figure 6: Notation for the next-to-leading order diagrams contributing to the $B \rightarrow V\gamma$ decay from \mathcal{Q}_1 (the diagram with the photon emitted from the other propagator in the quark loop is included implicitly). The extra gluon can be attached to any pair of circles (which might be identical). $(n7)$, for $n = 1-6$, represents the four diagrams for which the external photon and internal gluon are attached to either the quark or antiquark in the loop.

4 Factorisation at One-Loop Order for the Four-Quark Operator \mathcal{Q}_1

In this section we repeat the heuristic arguments with \mathcal{Q}_1 as the weak operator. For the soft divergences which are present in diagrams in which the additional gluon is attached to two external lines, the cancellation occurs in the standard way, exactly as described in section 3.1 and we don't discuss them any further. For the collinear divergences, we demonstrate below that they also cancel, but the pattern of cancellation is different in detail from that in section 3. Moreover the cancellation occurs even if we keep higher-twist contributions such as m_c^2/m_b^2 or $2q_2 \cdot k/m_b^2$ in the quark-loop. This is consistent with the arguments based on collinear Ward identities presented in appendix B.

The notation for the next-to-leading order diagrams is similar to that in our discussion of the contributions from \mathcal{Q}_8 . We denote by (ij) the diagrams in which the external photon is emitted from either of the two propagators in the quark loop and the internal gluon is attached to circles i and j . By $(n7)$ we mean the sum of the diagrams with one end of the gluon attached to either the quark or antiquark in the loop.

4.1 Divergences from the Region Collinear to q_2

4.1.1 Neglecting terms of $O(m_c^2/m_b^2)$

We now repeat the steps of section 3.2.1 for the operator \mathcal{Q}_1 with the photon emitted from the internal loop, beginning with the simpler case in which we neglect m_c . As before we start with diagram (12) (see fig. 7) for which the expression in this collinear region is now

$$(12) = 2ig^2 \left(C_F - \frac{C_A}{2} \right) \mathcal{A}_1^{(0)} \int \frac{d^4 l}{(2\pi)^4} \frac{\bar{x} - \xi}{\xi} \frac{1}{l^2} \frac{1}{(\bar{x}q_2 - l)^2}, \quad (49)$$

where $\mathcal{A}_1^{(0)}$ is the amplitude at tree level. This is no longer cancelled by the corresponding contribution from diagram (23) (see fig. 7) which is now given by

$$(23) = -2ig^2 \left(C_F - \frac{C_A}{2} \right) \mathcal{A}_1^{(0)} \int \frac{d^4l}{(2\pi)^4} \frac{\bar{x} - \xi}{\xi} \frac{x}{x + \xi} \frac{1}{l^2} \frac{1}{(\bar{x}q_2 - l)^2}. \quad (50)$$

Using eq. (36), we can see that the contribution $(2V)'$ to $\Phi^{b\bar{q}'}^{(0)} \otimes T_8^{(0)} \otimes \Phi^{q\bar{q}'}^{(1)}$ cancels the abelian component of these two diagrams:

$$(2V)' = 2ig^2 C_F \mathcal{A}_1^{(0)} \int \frac{d^4l}{(2\pi)^4} \frac{\bar{x} - \xi}{x + \xi} \frac{1}{l^2} \frac{1}{(\bar{x}q_2 - l)^2}. \quad (51)$$

Indeed the abelian component of diagram (12) is cancelled by the contribution to $(2V)'$ coming from the first delta function in eq. (36) and similarly the collinear divergence in diagram (23) is cancelled by the contribution from the second delta function. This simple observation will be important when we generalise the discussion to include corrections of $O(m_c^2/m_b^2)$. Thus we have

$$(12) + (23) - (2V)' = -ig^2 C_A \mathcal{A}_1^{(0)} \int \frac{d^4l}{(2\pi)^4} \frac{\bar{x} - \xi}{x + \xi} \frac{1}{l^2} \frac{1}{(\bar{x}q_2 - l)^2}. \quad (52)$$

In the case where we neglect the mass of the charm quark, the non-abelian contribution in eq. (52) is cancelled by diagram (26). There are no collinear divergences from the sum of diagrams (27).

Similarly, the expressions for diagrams (34) (which is unchanged from that in eq. (40)), (14) and $(4V)'$ (see eq. (37)) are now

$$(34) = 2ig^2 \left(C_F - \frac{C_A}{2} \right) \mathcal{A}_1^{(0)} \int \frac{d^4l}{(2\pi)^4} \frac{x - \xi}{\xi} \frac{1}{l^2} \frac{1}{(xq_2 - l)^2}, \quad (53)$$

$$(14) = -2ig^2 \left(C_F - \frac{C_A}{2} \right) \mathcal{A}_1^{(0)} \int \frac{d^4l}{(2\pi)^4} \frac{x}{\xi} \frac{1}{l^2} \frac{1}{(xq_2 - l)^2} \quad \text{and} \quad (54)$$

$$(4V)' = -2ig^2 C_F \mathcal{A}_1^{(0)} \int \frac{d^4l}{(2\pi)^4} \frac{1}{l^2} \frac{1}{(xq_2 - l)^2}, \quad (55)$$

so that the abelian component cancels and

$$(14) + (34) - (4V)' = ig^2 C_A \mathcal{A}_1^{(0)} \int \frac{d^4l}{(2\pi)^4} \frac{1}{l^2} \frac{1}{(\bar{x}q_2 - l)^2}. \quad (56)$$

This contribution is cancelled by diagram (46). If we neglect the mass of the charm quark there are no collinear divergences from the sum of the diagrams (47).

Thus the collinear divergences from the region of phase space in which l is parallel to q_2 either cancel or are absorbed into the vector meson's distribution amplitude.

4.1.2 Including terms of $O(m_c^2/m_b^2)$

In this subsection we demonstrate that the collinear divergences cancel, even if we include the corrections of $O(m_c^2/m_b^2)$. The additional complication is that the integral over momentum in the charm-quark loop now depends on whether the outgoing momentum in the gluon attached to the loop is $xq_2 - k$ (as in diagram (12) in fig. 7 for example) or $xq_2 - k + l$ (as in diagram (23) in fig. 7 for example). We will consider diagrams (27) and (47), in which two gluons are

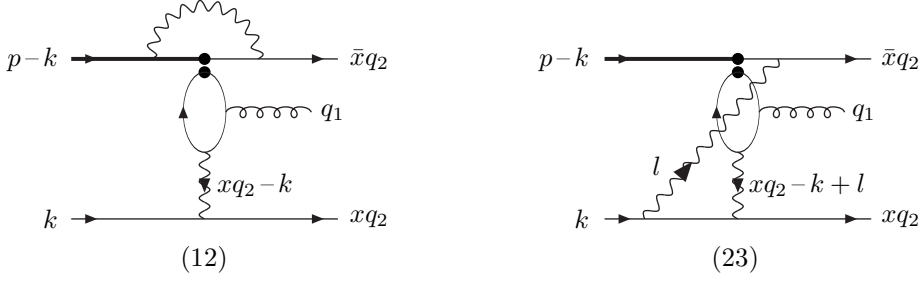


Figure 7: One-loop diagrams (12) and (23) contributing to corrections to the matrix element of Q_1 . The corresponding diagrams in which the photon is emitted from the other propagator in the quark loop are to be considered implicitly included.

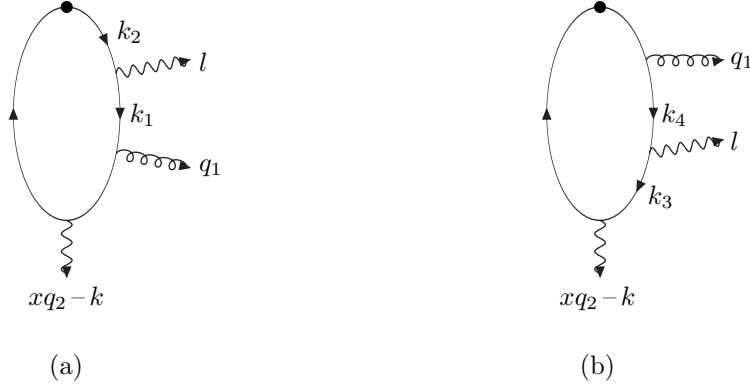


Figure 8: Two of the attachments of the gluon of momentum l onto the quark loop (see text).

attached to the charm-quark loop, separately. In order to distinguish between the two types of contribution we write

$$\mathcal{A}_1^{(0)}(x) = \frac{1}{x} I_1(x), \quad (57)$$

where the x dependence in $I_1(x)$ comes from the integral over the loop-momentum in the quark loop and is exhibited explicitly in eqs. (23)–(26). If we neglect m_c^2/m_b^2 , then $I_1(x)$ is independent of x , which leads to the vanishing of some contributions, such as (27) and (47). Since now we do not neglect these effects, we must distinguish the two type of one-loop corrections, corresponding to $I_1(x)$ and $I_1(x + \xi)$ respectively; in the latter case the factor is in the integrand of the l integration. We now demonstrate that neither type of contribution contains collinear divergences.

We start by considering the terms proportional to $I_1(x)$ arising from diagrams with a gluon attached to the outgoing quark line with momentum $\bar{x}q_2$. The corresponding diagrams are (12), $(2V)'$ and (27). Repeating the steps in section 4.1.1 we find

$$(12) - (2V)' = -ig^2 C_A \frac{I_1(x)}{x} \int \frac{d^4 l}{(2\pi)^4} \frac{\bar{x} - \xi}{\xi} \frac{1}{l^2} \frac{1}{(\bar{x}q_2 - l)^2}. \quad (58)$$

The remaining contribution of this type comes from diagrams (27). The numerator of the light-quark propagator has a factor of $2(\bar{x} - \xi)q_2^\mu \simeq 2(\bar{x} - \xi)/\xi l^\mu$, where μ is the Lorentz index of the gluon with momentum l . Consider first the diagram in fig. 8 (a), for which $l = k_2 - k_1$. Using the Ward identity

$$\frac{1}{\not{k}_1 - m} \{k_2 - k_1\} \frac{1}{\not{k}_2 - m} = \frac{1}{\not{k}_1 - m} - \frac{1}{\not{k}_2 - m} \quad (59)$$

inside the quark loop, we readily see that the integral over the quark loop can be reduced to ones with only three quark propagators. The first term on the right-hand side of eq. (59) gives a contribution proportional to $I_1(x)$. Similarly consider the insertion of the gluon as in fig. 8 (b) and the Ward identity

$$\frac{1}{\not{k}_3 - m} \{\not{k}_4 - \not{k}_3\} \frac{1}{\not{k}_4 - m} = \frac{1}{\not{k}_3 - m} - \frac{1}{\not{k}_4 - m}. \quad (60)$$

The first term on the right-hand side of eq. (60) cancels the second term of eq. (59), and the second term of eq. (60) gives a contribution proportional to $I_1(x + \xi)$. These arguments can be generalized to include all the insertions of the photon and gluon onto the quark loop. The term proportional to $I_1(x)$ precisely cancels the contribution from $(12) - (2V)'$ in eq. (58).

The cancellation of the terms with integrands proportional to $I_1(x + \xi)$ in diagrams with the gluon with momentum l attached to the external light quark with momentum $\bar{x}q_2$ proceeds in a similar way. The corresponding contributions are as follows:

$$\begin{aligned} (23) - (2V)' &= ig^2 C_A \int \frac{d^4 l}{(2\pi)^4} \frac{\bar{x} - \xi}{\xi} \frac{I_1(x + \xi)}{x + \xi} \frac{1}{l^2} \frac{1}{(\bar{x}q_2 - l)^2}, \\ (26) &= ig^2 C_A \int \frac{d^4 l}{(2\pi)^4} \frac{\bar{x} - \xi}{x} \frac{I_1(x + \xi)}{x + \xi} \frac{1}{l^2} \frac{1}{(\bar{x}q_2 - l)^2}, \\ (27) &= -ig^2 C_A \int \frac{d^4 l}{(2\pi)^4} \frac{\bar{x} - \xi}{\xi} \frac{I_1(x + \xi)}{x} \frac{1}{l^2} \frac{1}{(\bar{x}q_2 - l)^2}, \end{aligned}$$

so that

$$(23) - (2V)' + (26) + (27) = 0 \quad (61)$$

and all the mass singularities cancel as required.

The cancellation of the mass singularities from the diagrams in which the gluon with momentum l is attached to the light antiquark with momentum xq_2 proceeds in a very similar way, except that now we have factors $I_1(x)$ and $I_1(x - \xi)$. For the terms with a factor $I_1(x)$ the contributions are:

$$(34) - (4V)' = -ig^2 C_A \frac{I_1(x)}{x} \int \frac{d^4 l}{(2\pi)^4} \frac{x - \xi}{\xi} \frac{1}{l^2} \frac{1}{(xq_2 - l)^2}, \quad (62)$$

$$(46) = -ig^2 C_A \frac{I_1(x)}{x} \int \frac{d^4 l}{(2\pi)^4} \frac{1}{l^2} \frac{1}{(xq_2 - l)^2}, \quad (63)$$

$$(47) = ig^2 C_A \frac{I_1(x)}{x} \int \frac{d^4 l}{(2\pi)^4} \frac{x}{\xi} \frac{1}{l^2} \frac{1}{(xq_2 - l)^2}, \quad (64)$$

$$(65)$$

which sum to zero, and for the terms with a factor $I_1(x - \xi)$ in the integrand we have

$$(14) - (4V)' = -(47) = ig^2 C_A \int \frac{d^4 l}{(2\pi)^4} \frac{I_1(x - \xi)}{\xi} \frac{1}{l^2} \frac{1}{(xq_2 - l)^2}. \quad (66)$$

Thus again, all the collinear divergences from the region in which a gluon's momentum is parallel to q_2 cancel.

4.1.3 Divergences from the Region Collinear to k

For the kinematical situation considered in ref. [6], in which we keep m_c^2/m_b^2 but neglect $q_2 \cdot k/m_b^2$, the cancellation of the mass singularities from the region in which a gluon is collinear to k follows exactly as in the case of the operator \mathcal{Q}_8 discussed in section 4.1.3 (see equations (45) - (48)).

This concludes the demonstration of the cancellation of mass singularities. However it is also instructive to ask whether they would have cancelled if we had not neglected $q_2 \cdot k/m_b^2$. We now rewrite the amplitude at lowest order as

$$\mathcal{A}_1^{(0)} = \frac{1}{xk_+} I_2(x, k_+), \quad (67)$$

where $I_2(x, k_+) = k_+ I_1(x, k_+)$ and the k_+ dependence in eq. (57) and subsequent equations was implicit. For all the discussion above, the k_+ dependence in $I_1(x)$ was contained in a simple overall factor of $1/k_+$. Now, if we keep terms of $O(q_2 \cdot k/m_b^2)$, we have two types of term in the integrands of the loop integrations, those proportional to $I_2(x, k_+)$ and those proportional to $I_2(x, (1-\sigma)k_+)$. We now demonstrate that the corresponding mass singularities cancel also in this case.

The distribution amplitude of the initial state is defined by

$$\Phi_{\alpha\beta}^{b\bar{q}'}(\tilde{k}_+) = \int dz_- e^{i\tilde{k}_+ z_-} \langle 0 | \bar{q}'_{\beta}(z) [z, 0] b_{\alpha}(0) | b(p) \bar{q}'(k) \rangle |_{z_+, z_{\perp}=0}, \quad (68)$$

so that at tree level (see eq. (18))

$$\Phi_{\alpha\beta}^{b\bar{q}'}{}^{(0)}(\tilde{k}_+) = 2\pi\delta(k_+ - \tilde{k}_+) \bar{v}_{\beta}(k) u_{\alpha}(p - k), \quad (69)$$

where v and u are the free spinor wave functions of the light antiquark and the b -quark respectively. In the collinear region which we are considering here, the one-loop correction from the diagram in fig. 5(c) can be written in the form

$$\Phi_{(c)\alpha\beta}^{b\bar{q}'(1)}(\tilde{k}_+) = 2ig^2 C_F \bar{v}_{\beta}(k) u_{\alpha}(p) \int \frac{d^4 l}{(2\pi)^4} \frac{(1-\sigma)}{\sigma} \left\{ \delta(\tilde{k}_+ - k_+) - \delta(\tilde{k}_+ - (1-\sigma)k_+) \right\} \frac{1}{l^2(k-l)^2}, \quad (70)$$

where the subscript (c) denotes that this is the contribution from the diagram of fig. 5(c), and the superscript (1) that it is a one-loop contribution. $\Phi^{b\bar{q}'(1)} \otimes T^{(0)} \otimes \Phi^{q\bar{q}'(0)}$ is therefore

$$(3B)' = 2ig^2 C_F \frac{1}{xk_+} \int \frac{d^4 l}{(2\pi)^4} \frac{1}{\sigma} \left\{ (1-\sigma)I_2(x, k_+) - I_2(x, (1-\sigma)k_+) \right\} \frac{1}{l^2(k-l)^2}. \quad (71)$$

The results in section 3.2.2 are now modified as follows:

$$(23) = -2ig^2 \left(C_F - \frac{C_A}{2} \right) \frac{1}{xk_+} \int \frac{d^4 l}{(2\pi)^4} \frac{I_2(x, (1-\sigma)k_+)}{\sigma} \frac{1}{l^2(k-l)^2}, \quad (72)$$

$$(34) = 2ig^2 \left(C_F - \frac{C_A}{2} \right) \frac{1}{xk_+} \int \frac{d^4 l}{(2\pi)^4} \frac{1-\sigma}{\sigma} \frac{I_2(x, k_+)}{l^2(k-l)^2}, \quad (73)$$

$$(36) = -ig^2 C_A \frac{1}{xk_+} \int \frac{d^4 l}{(2\pi)^4} \frac{I_2(x, k_+)}{l^2(k-l)^2}. \quad (74)$$

Finally we have to consider the diagrams (37) which no longer vanish when we include the terms of $O(q_2 \cdot k/m_b^2)$. Using the Ward identity in eq. (59) the contribution from these diagrams is readily found to be:

$$(37) = ig^2 C_A \frac{1}{xk_+} \int \frac{d^4 l}{(2\pi)^4} \frac{I_2(x, k_+) - I_2(x, (1-\sigma)k_+)}{\sigma} \frac{1}{l^2 (k-l)^2}. \quad (75)$$

Thus we have

$$(23) + (34) + (36) + (37) = (3B)', \quad (76)$$

so that there are no mass singularities remaining in the hard-scattering amplitude.

5 Conclusions

In this paper, we have studied the radiative decays $B \rightarrow V\gamma$ (where $V = \rho, K^*$) in the framework of QCD factorisation. We focused on spectator interactions, where the most significant contributions come from the chromomagnetic operator \mathcal{Q}_8 and the four-quark operator \mathcal{Q}_1 . These contributions had previously been considered explicitly at leading order [6, 7], and they exhibit similar features to the purely radiative decays $B \rightarrow \gamma\ell\nu$ ($\gamma\gamma, \gamma\ell^+\ell^-$) that we have already considered [11, 12]. However, the presence of two light-cone distribution amplitudes (those of the B and vector mesons) leads to technical and conceptual modifications.

We have performed an explicit next-to-leading-order computation of the contribution from \mathcal{Q}_8 in the heavy-quark limit $m_b \rightarrow \infty$ (specifically we have calculated all the terms containing mass singularities and large logarithms), and we showed that the spectator interactions factorise, i.e. they can be written as the convolution of a hard-scattering kernel, computable in perturbation theory, and of two light-cone distribution amplitudes (one for each meson) describing soft physics. The explicit results are presented in appendix A. By studying the soft and collinear regions of the loop momentum, we can understand the factorisation of mass singularities using a heuristic argument (presented in section 3). The same argument can be applied to the 4-quark operator \mathcal{Q}_1 , so that its contribution to spectator interactions are also expected to factorise at next-to-leading order. In appendix B we use the collinear Ward identity to demonstrate the factorisation of mass singularities at next-to-leading order for all the weak operators contributing to $B \rightarrow V\gamma$ decays.

This success of QCD factorisation for $B \rightarrow V\gamma$ spectator interactions leaves several questions open. First, the presence of an intermediate scale $\sqrt{\Lambda_{QCD}m_b}$, corresponding to the virtuality of the exchanged gluon, yields large (Sudakov) logarithms at all orders of perturbation theory. The latter could be resummed using renormalization-group arguments within the Soft-Collinear Effective Theory [13, 14, 8]; for the resummation in purely radiative decays see refs. [11, 12]. However, the mixing of the operators and hence the subsequent resummation are much more intricate than in the case of $b \rightarrow u$ transitions⁵. We have only considered twist-2 distribution amplitudes for both mesons: higher-twist distribution amplitudes deserve a separate study. One could also consider the interesting decay $B \rightarrow V\ell^+\ell^-$, where the light vector meson is longitudinally polarized and the lepton pair has a small invariant mass. In ref. [7], the spectator interactions were analysed at leading order: they receive contributions from additional diagrams to those considered here, involving (in particular) the second leading-twist B -meson distribution amplitude Φ_-^B . Of course, one would also like to understand in detail hard spectator interactions in two-body nonleptonic B -decays.

⁵We thank M. Neubert for instructive discussions on this point.

Acknowledgements

We thank Gerhard Buchalla and Matthias Neubert for helpful comments and discussion.

C.T.S. acknowledges partial support from PPARC through the grant PPA/G/O/1998/00525. S.D.G. acknowledges partial support from EU-RTN contract EURIDICE (HPRN-CT-2002-00311).

A Contribution of \mathcal{Q}_8 at one loop

In this appendix we present the results from explicit evaluation of the Feynman diagrams at one-loop order for the chromomagnetic operator \mathcal{Q}_8 . Specifically we exhibit the mass singularities and all the large logarithms. We denote as (ij) the contribution from the diagram where i and j are connected with a gluon in Fig. 3. Each diagram's contribution is given in units of $\alpha_s/(4\pi)\mathcal{A}_8^{(0)}$. We use dimension regularisation to regulate both the ultraviolet and infrared divergences, but introduce separate scales for the two cases.

A.1 Abelian Component

We start by considering those diagrams which have an Abelian component, i.e. which have a component proportional to C_F .

A.1.1 Contributions to $\mathcal{A}_8^{(1)}$

There are four diagrams with a gluon which links an initial-state quark with a final-state one:

$$(12) = \left(C_F - \frac{C_A}{2}\right) \left[-\frac{1}{2} \log^2 \frac{M_B^2}{\mu_{\text{IR}}^2} - 2 \log \bar{x} \log \frac{M_B^2}{\mu_{\text{IR}}^2} \right] \quad (77)$$

$$(14) = \left(C_F - \frac{C_A}{2}\right) \left[\frac{1}{2} \log^2 \frac{M_B^2}{\mu_{\text{IR}}^2} + (2 \log x - 2) \log \frac{2(k \cdot q_2)}{\mu_{\text{IR}}^2} - \log^2 \frac{2(k \cdot q_2)}{M_B^2} \right] \quad (78)$$

$$(23) = \left(C_F - \frac{C_A}{2}\right) \left[\log^2 \frac{2(k \cdot q_2)}{\mu_{\text{IR}}^2} + 2 \log \bar{x} \log \frac{2(k \cdot q_2)}{\mu_{\text{IR}}^2} \right] \quad (79)$$

$$(34) = \left(C_F - \frac{C_A}{2}\right) \left[-\log^2 \frac{2(k \cdot q_2)}{\mu_{\text{IR}}^2} + (-2 \log x + 4) \log \frac{2(k \cdot q_2)}{\mu_{\text{IR}}^2} - \log \frac{2(k \cdot q_2)}{\mu_{\text{UV}}^2} \right]. \quad (80)$$

One may also link the external lines of the same hadron, yielding

$$(13) = C_F \left[-\frac{1}{2} \log^2 \left(-\left(\frac{2k \cdot q_2}{M_B \mu_{\text{IR}}} \right)^2 \right) \right]$$

$$(24) = 0$$

at leading twist.

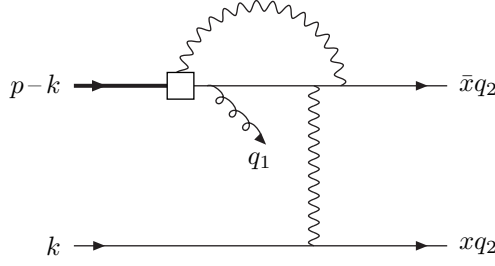


Figure 9: An additional diagram, D , which contains a large logarithm and which is not included in the set of diagrams $\{(ij)\}$ defined in section 3.

When an external line is linked to the internal quark propagator one gets

$$\begin{aligned}
(15) &= 0 \\
(25) &= C_F \left[2 \log \frac{M_B^2}{\mu_{\text{IR}}^2} - \log \frac{M_B^2}{\mu_{\text{UV}}^2} \right] \\
(35) &= 0 \\
(45) &= C_F \log \frac{2(k \cdot q_2)}{\mu_{\text{IR}}^2} \left[2 \frac{1}{x} \log \bar{x} + 2 \right]
\end{aligned}$$

There are also contributions from the wave function renormalization of the external lines

$$\begin{aligned}
(11) &= C_F \left[\frac{1}{2} \log \frac{M_B^2}{\mu_{\text{UV}}^2} + \log \frac{M_B^2}{\mu_{\text{IR}}^2} \right] \\
(22) &= 0 \equiv C_F \left[\frac{1}{2} \log \frac{\mu_{\text{IR}}^2}{\mu_{\text{UV}}^2} \right] \\
(33) &= 0 \equiv C_F \left[\frac{1}{2} \log \frac{\mu_{\text{IR}}^2}{\mu_{\text{UV}}^2} \right] \\
(44) &= 0 \equiv C_F \left[\frac{1}{2} \log \frac{\mu_{\text{IR}}^2}{\mu_{\text{UV}}^2} \right] \\
(55) &= C_F \left[\log \frac{M_B^2}{\mu_{\text{UV}}^2} \right]
\end{aligned}$$

where the vanishing values correspond to massless tadpole diagrams in dimensional regularisation.

Finally, there is a contribution containing large logarithms that cannot be obtained by adding one gluon to the leading-twist tree-level diagram and is therefore not included in the set $\{(ij)\}$ defined in section 3. We denote it by D and exhibit it in fig. 9; its contribution to the amplitude is:

$$D = (C_F - C_A/2) \frac{\bar{x}}{x} \left[-2 \log \left(-\frac{2k \cdot q_2}{M_B^2} \right) - \log \left(-\frac{M_B^2}{\mu_{\text{UV}}^2} \right) \right]. \quad (81)$$

The other diagrams not included in the set $\{(ij)\}$ do not give large logarithms when μ_{UV} is set equal to M_B .

A.1.2 Distribution amplitudes

We consider now the contribution to the distribution amplitudes convoluted with the lowest-order kernel, $\Phi^{b\bar{q}'}(1) \otimes T_8^{(0)} \otimes \Phi^{q\bar{q}'}(0) + \Phi^{b\bar{q}'}(0) \otimes T_8^{(0)} \otimes \Phi^{q\bar{q}'}(1)$. As explained in section 3, we

denote the diagrams in a similar way to those for the amplitude. Once again we use dimensional regularisation to regulate both infrared and ultraviolet divergences. The infrared scale, μ_{IR} , is the same for the matrix elements and the distribution amplitudes. The ultraviolet scale is different in the two cases however: for the matrix elements μ_{UV} corresponds to the renormalization scale μ_R , whereas for the distribution amplitudes ν_{UV} corresponds to the factorisation scale μ_F (see ref. [11] for further discussion). In agreement with our definition of Φ^H , we use the HQET Lagrangian when a gluon is connected to the b -quark.

We can link an external line to the path-ordered exponential of one distribution amplitude

$$\begin{aligned}
(1B)' &= C_F \left[-\frac{1}{2} \log^2 \frac{2k_+^2}{\nu_{\text{UV}}^2} \right] \\
(2V)' &= 0 \equiv C_F \left[2 \log \frac{\nu_{\text{UV}}^2}{\mu_{\text{IR}}^2} \right] \\
(3B)' &= 0 \equiv C_F \left[2 \log \frac{\nu_{\text{UV}}^2}{\mu_{\text{IR}}^2} \right] \\
(4V)' &= C_F \log \frac{\nu_{\text{UV}}^2}{\mu_{\text{IR}}^2} \left[2 \frac{1}{x} \log \bar{x} + 2 \right].
\end{aligned}$$

We can also link two external lines

$$\begin{aligned}
(13)' &= C_F \left[-\frac{1}{2} \log^2 \left(- \left(\frac{2k \cdot q_2}{M_B \mu_{\text{IR}}} \right)^2 \right) \right] \\
(24)' &= 0
\end{aligned}$$

There are also contributions due to the wave function renormalization for external lines

$$\begin{aligned}
(11)' &= C_F \left[\log \frac{\nu_{\text{UV}}^2}{\mu_{\text{IR}}^2} \right] \\
(22)' &= 0 \equiv C_F \left[\frac{1}{2} \log \frac{\mu_{\text{IR}}^2}{\nu_{\text{UV}}^2} \right] \\
(33)' &= 0 \equiv C_F \left[\frac{1}{2} \log \frac{\mu_{\text{IR}}^2}{\nu_{\text{UV}}^2} \right] \\
(44)' &= 0 \equiv C_F \left[\frac{1}{2} \log \frac{\mu_{\text{IR}}^2}{\nu_{\text{UV}}^2} \right]
\end{aligned}$$

where the vanishing values correspond to massless tadpole diagrams in dimensional regularisation.

We could also try to link two points of the same path-ordered exponential. These diagrams involve the propagator associated with $A^+(\alpha z)A^+(\beta z)$ or $A^-(\alpha z)A^-(\beta z)$, which vanishes in the Feynman gauge.

A.2 Remaining Nonabelian Components

We now evaluate the one-loop contributions to $\mathcal{A}_8^{(1)}$ whose colour factor is proportional to C_A .

A.2.1 Diagrams with one Three-Gluon Vertex

The contributions from diagrams in which a gluon links an external quark line to the gluon one through a three-gluon vertex are as follows:

$$\begin{aligned}
(16) &= C_A \left[-\frac{1}{2} \log^2 \frac{2(k \cdot q_2)}{M_B^2} + \left(-\frac{5}{4} + \log x \right) \log \frac{2(k \cdot q_2)}{M_B^2} - \left(\frac{1}{2x} + 2 \right) \log \frac{M_B^2}{\mu_{\text{UV}}^2} \right] \\
(26) &= C_A \times \frac{\bar{x}}{x} \left[\frac{1}{2} \left(1 - \frac{\log \bar{x}}{x} \right) \log \frac{2(k \cdot q_2)}{M_B^2} - \log \frac{2(k \cdot q_2)}{\mu_{\text{IR}}^2} + \frac{1}{8} \log \frac{M_B^2}{\mu_{\text{UV}}^2} \right], \\
(36) &= C_A \left[-\frac{3}{2} \log \frac{2(k \cdot q_2)}{\mu_{\text{UV}}^2} + 2 \log \frac{2(k \cdot q_2)}{\mu_{\text{IR}}^2} \right],
\end{aligned}$$

keeping in mind that (46) is the same diagram as (36).

In the case of the internal quark propagator, we get

$$(56) = C_A \left[\left(-\frac{1}{2x} - \frac{3}{4} - \frac{1+x}{2x^2} \log \bar{x} \right) \log \frac{2(k \cdot q_2)}{M_B^2} + \left(-\frac{5}{8x} - \frac{11}{8} \right) \log \frac{M_B^2}{\mu_{\text{UV}}^2} \right].$$

A.2.2 Diagrams for the Gluonic Vacuum Polarization

The gluonic wave function renormalization yields

$$(66) = \left[\frac{2}{3} N_f - \frac{5}{3} C_A \right] \log \frac{2(k \cdot q_2)}{\mu_{\text{UV}}^2}.$$

A.2.3 Diagrams with two Gluons attached to \mathcal{Q}_8

We can also attach two gluons to the vertex with the operator \mathcal{Q}_8 . One of them interacts with the spectator quark, whereas the second is attached elsewhere.

When one of the gluons is attached to an external line, we obtain

$$\begin{aligned}
(17) &= C_A \times \frac{5}{4x} \log \frac{M_B^2}{\mu_{\text{UV}}^2} \\
(27) &= C_A \times \frac{\bar{x}}{x} \left[-\frac{1}{2} \log \frac{M_B^2}{\mu_{\text{UV}}^2} + \log \frac{M_B^2}{\mu_{\text{IR}}^2} \right] \\
(37) &= C_A \times (-1) \log \frac{2(k \cdot q_2)}{\mu_{\text{IR}}^2}
\end{aligned}$$

where (37) and (47) denote the same diagram.

The result for diagram (57) obtained by attaching one of the gluons to the internal quark propagator is

$$(57) = C_A \times \frac{\bar{x}}{4x} \log \frac{M_B^2}{\mu_{\text{UV}}^2}$$

and for diagram (67) in which the gluon is attached the internal gluon propagator is

$$(67) = C_A \times \frac{3}{2} \log \frac{2(k \cdot q_2)}{\mu_{\text{UV}}^2}.$$

A.3 One-loop results

We now combine the results presented above to obtain the large logarithms at NLO in the amplitude, in $\Phi^B \otimes T_8 \otimes \Phi_\perp$ and hence finally in the hard-scattering kernel. These next-to-leading-order results contain logarithms of ratios of the scales μ_R , μ_F , M_B and $q_2 \cdot k$. Following ref. [11, 12], the natural choices for the renormalisation and factorisation scales are

$$\mu_R = O(M_B) \quad \mu_F = \mu_i = O(q_2 \cdot k) \quad (82)$$

But even with this choice, large logarithms will remain due to the presence of three distinct scales. Therefore, in presenting our results we focus on the mass singularities and large logarithms. The amplitude up to one-loop order is:

$$\begin{aligned} \mathcal{A}_8^{(0+1)}(\mu_R = M) &= \mathcal{A}_8^{(0)}(\mu_R = \mu_i) \\ &\times \left[1 + \frac{\alpha_s}{4\pi} \left\{ C_F \left[\frac{7}{2} \log \frac{\mu_i^2}{\mu_{\text{IR}}^2} + \left(\frac{2}{x} \log \bar{x} + 2 \right) \log \frac{\mu_i^2}{\mu_{\text{IR}}^2} - \frac{1}{2} \log \left(- \left(\frac{\mu_i^2}{M_B \mu_{\text{IR}}} \right)^2 \right) - \log^2 \frac{\mu_i^2}{M_B^2} \right. \right. \right. \\ &\left. \left. \left. + \left[2 \log \bar{x} - 2 \frac{\bar{x}}{x} - \frac{5}{2} \right] \log \frac{\mu_i^2}{M_B^2} \right] + C_A \left[- \log \frac{\bar{x}}{x} - \frac{1}{x^2} \log \bar{x} \right] \log \frac{\mu_i^2}{M_B^2} + \dots \right\} \right] + O(\alpha_s^2) \quad (83) \end{aligned}$$

where $\mathcal{A}_8^{(0)}(\mu_R)$ denotes the tree-level matrix element with μ_R as the scale of the strong coupling constant, and the ellipses denote terms without large logarithms.

The contribution from the distribution amplitudes is

$$\begin{aligned} [\Phi^H \otimes T_8 \otimes \Phi^V]^{(0+1)}(\mu_F = \mu_i) &= \mathcal{A}_8^{(0)} \times \left[1 + \frac{\alpha_s}{4\pi} C_F \times \right. \\ &\left. \left[\frac{7}{2} \log \frac{\mu_i^2}{\mu_{\text{IR}}^2} + \left(\frac{2}{x} \log \bar{x} + 2 \right) \log \frac{\mu_i^2}{\mu_{\text{IR}}^2} - \frac{1}{2} \log \left(- \left(\frac{\mu_i^2}{M_B \mu_{\text{IR}}} \right)^2 \right) - \frac{1}{2} \log^2 \frac{\mu_i^2}{M_B^2} \right] \right] + O(\alpha_s^2). \quad (84) \end{aligned}$$

The one-loop result for the hard-scattering kernel at next-to-leading order is therefore:

$$\begin{aligned} T_8^{(0+1)}(\tilde{k}_+, u; \mu_R = M, \mu_F = \mu_i) &= T_8^{(0)}(\tilde{k}_+, u; \mu_R = \mu_i) \times \left[1 + \frac{\alpha_s}{4\pi} \times \right. \\ &\left. \left\{ - \frac{C_F}{2} \log^2 \frac{\mu_i^2}{M_B^2} + C_F \left[2 \log \bar{x} - 2 \frac{\bar{x}}{x} - \frac{5}{2} \right] \log \frac{\mu_i^2}{M_B^2} + C_A \left[- \log \frac{\bar{x}}{x} - \frac{1}{x^2} \log \bar{x} \right] \log \frac{\mu_i^2}{M_B^2} + \dots \right\} \right] \\ &+ O(\alpha_s^2) \quad (85) \end{aligned}$$

where $T_8^{(0)}(\tilde{k}_+, u; \mu_R)$ denotes the tree-level hard-scattering kernel with μ_R as the scale of the strong coupling constant, and the ellipses denote terms without large logarithms. The key point is, of course, that there are no mass singularities in the expression for T_8 .

B Cancellation of Collinear Divergences and the Collinear Ward Identity

In this appendix we show that the cancellations of collinear divergences demonstrated in sections 3 and 4 are a general consequence of the collinear Ward identity and hold for all the

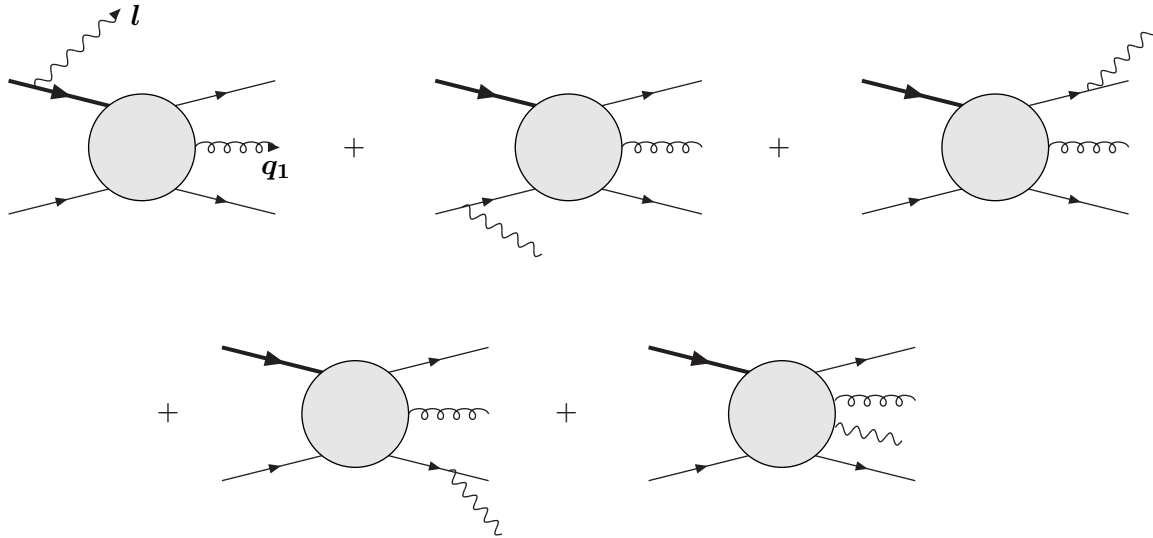


Figure 10: Amplitude for the auxiliary process $b\bar{q} \rightarrow q\bar{q}\gamma + \text{gluon}$. The spring represents the photon (with momentum q_1) and the curly line the gluon (with outgoing momentum l). The first four diagrams are those in which the final-state gluon is attached to one of the four external quark lines. The fifth diagram represents all the remaining ways in which the final-state gluon can be attached.

weak operators contributing to $B \rightarrow V\gamma$ decays⁶. It will be useful to consider (in perturbation theory) the on-shell amplitude $b\bar{q}' \rightarrow q\bar{q}'\gamma + \text{gluon}$, where the momentum of the gluon is l . We represent this amplitude by the graphs in Fig. 10, exhibiting explicitly the diagrams in which the gluon is attached to an external quark line. We write this amplitude as $\varepsilon_g^\mu(l)\mathcal{M}_\mu$, where ε_g is the polarization vector of the gluon. The Ward Identity we wish to exploit is

$$l^\mu \mathcal{M}_\mu = 0. \quad (86)$$

The process we are actually studying in the evaluation of the one-loop contributions to the hard-scattering kernels is $b\bar{q}' \rightarrow q\bar{q}'\gamma$, where the momenta of the incoming b -quark and light antiquark are $q_1 + q_2 - k$ and k respectively and those of the outgoing quark and antiquark are $\bar{x}q_2$ and xq_2 . We denote this amplitude at lowest order in perturbation theory by $\mathcal{A}^{(0)}(x, k)$, without specifying which operator mediates the weak transition. The corresponding hard-scattering kernel is written as $T^{(0)}$, where we suppress the spinor indices.

We start by the demonstration of the cancellation of collinear divergences from the region in which l is collinear to q_2 , $l \simeq \xi q_2$. It is convenient to use the identity in eq. (59) to represent the Ward identity (86) by Fig. 11. On the right-hand side we have eliminated the fermion propagator immediately to the left of the solid dot. Since the external particles are on-shell we can use the identity in Fig. 11 with the external wave functions amputated.

We now consider the identity in Fig. 11 with the external wave functions amputated, and with the momentum of the final state quark equal to $\bar{x}q_2 - l$. We multiply both sides of Fig. 11 by the factor

$$-2ig \frac{\bar{x} - \xi}{\xi} \frac{1}{l^2(\bar{x}q_2 - l)^2}, \quad (87)$$

⁶Similar arguments were presented in a different context in Ref. [23].

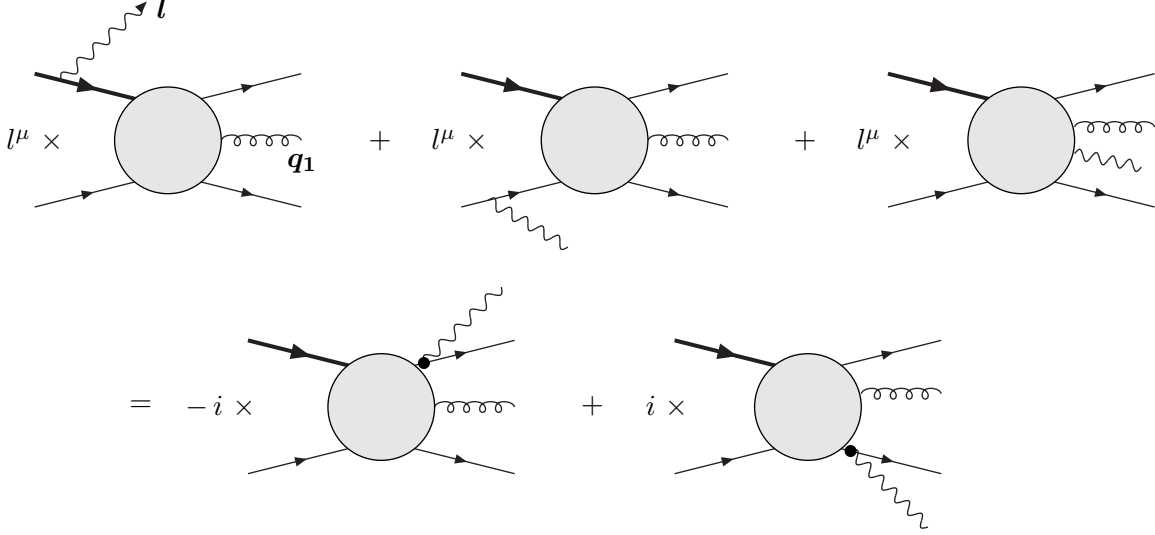


Figure 11: Representation of the Ward identity in eq. (86). The solid dot in the two diagrams on the right-hand side indicates that the gluon is attached with factor igT^a (but no γ -matrix) and the propagator to the left of the dot has been eliminated using eq. (59).

and the outgoing quark line by the colour matrix T^a (a is the colour label of the final-state gluon). Integrating over l (in the collinear region), on the left hand side we generate all the diagrams with a gluon attached to final-state quark line (i.e. the line denoted by 2), except for (22) and (24)⁷. From the identity in Fig. 11, we then immediately understand that for any operator the sum of these diagrams gives a contribution which can be written in terms of a convolution of the properties of the final state with the lowest-order amplitude. Specifically, Fig 11 gives

$$\sum_{n \neq 2,4} (2n) = 2ig^2 C_F \int \frac{d^4 l}{(2\pi)^4} \frac{\bar{x} - \xi}{\xi} \frac{\mathcal{A}^{(0)}(x, k) - \mathcal{A}^{(0)}(x + \xi, k)}{l^2(\bar{x}q_2 - l)^2} \quad (88)$$

$$= \Phi^{b\bar{q}'(0)} \otimes T^{(0)} \otimes \Phi_{(a)}^{q\bar{q}'(1)} \quad (89)$$

$$= (2V)', \quad (90)$$

where the second line follows from eq. (36). Here we have restored the external quark wave functions.

Following similar arguments and eq. (37) one also obtains

$$\sum_{n \neq 2,4} (4n) = 2ig^2 C_F \int \frac{d^4 l}{(2\pi)^4} \frac{x - \xi}{\xi} \frac{\mathcal{A}^{(0)}(x, k) - \mathcal{A}^{(0)}(x - \xi, k)}{l^2(xq_2 - l)^2} \quad (91)$$

$$= \Phi^{b\bar{q}'(0)} \otimes T^{(0)} \otimes \Phi_{(b)}^{q\bar{q}'(1)} \quad (92)$$

$$= (4V)'. \quad (93)$$

Finally one can use the same procedure for the collinear divergences from the region in which l is parallel to k ($l \simeq \sigma k$). In this case we use the identity in eq. (59) to eliminate the propagators

⁷Apart from the factor in eq. (87), we have set $(\bar{x}q_2 - l)^2 = 0$ everywhere, which is correct at leading twist.

to the right of the gluon vertex in the first two diagrams of Fig. 10, and obtain

$$\sum_{n \neq 1,3} (3n) = 2ig^2 C_F \int \frac{d^4 l}{(2\pi)^4} \frac{1-\sigma}{\sigma} \frac{\mathcal{A}^{(0)}(x, k) - \mathcal{A}^{(0)}(x, (1-\sigma)k)}{l^2(k-l)^2} \quad (94)$$

$$= \Phi_{(c)}^{b\bar{q}'(1)} \otimes T^{(0)} \otimes \Phi^{q\bar{q}'(0)} \quad (95)$$

$$= (3B)'. \quad (96)$$

Thus all the collinear divergences are absorbed into the light-cone distribution amplitudes for any of the weak operators \mathcal{Q}_i (the argument presented here considers all singularities from the collinear region, and includes in particular the soft-collinear modes discussed recently in refs. [24]). It is straightforward to verify that for \mathcal{Q}_8 , for which

$$A^{(0)}(x, k) \propto \frac{1}{\bar{x}k_+},$$

one recovers the results in section 3 and similarly for \mathcal{Q}_1 one recovers the results in 4.

References

- [1] F. Di Lodovico, hep-ex/0308045.
- [2] B. Aubert *et al.* [BABAR Collaboration], Phys. Rev. Lett. **92** (2004) 111801 [hep-ex/0306038].
- [3] M. A. Shifman and M. B. Voloshin, Sov. J. Nucl. Phys. **41** (1985) 120 [Yad. Fiz. **41** (1985) 187].
I. I. Y. Bigi, M. A. Shifman and N. Uraltsev, Ann. Rev. Nucl. Part. Sci. **47** (1997) 591 [hep-ph/9703290] and references therein.
- [4] M. Beneke, G. Buchalla, M. Neubert and C. T. Sachrajda, Phys. Rev. Lett. **83** (1999) 1914; Nucl. Phys. B **606** (2001) 245.
- [5] M. Beneke, G. Buchalla, M. Neubert and C. T. Sachrajda, Nucl. Phys. B **591** (2000) 313 [hep-ph/0006124].
- [6] S. W. Bosch and G. Buchalla, Nucl. Phys. B **621** (2002) 459 [hep-ph/0106081].
- [7] M. Beneke, T. Feldmann and D. Seidel, Nucl. Phys. B **612** (2001) 25 [hep-ph/0106067].
- [8] J. g. Chay and C. Kim, Phys. Rev. D **68** (2003) 034013 [hep-ph/0305033].
- [9] S. W. Bosch, hep-ph/0310317.
- [10] A. Ali and A. Y. Parkhomenko, Eur. Phys. J. C **23** (2002) 89 [hep-ph/0105302]. A. Ali and E. Lunghi, Eur. Phys. J. C **26** (2002) 195 [hep-ph/0206242].
- [11] S. Descotes-Genon and C. T. Sachrajda, Nucl. Phys. B **650** (2003) 356 [hep-ph/0209216].
- [12] S. Descotes-Genon and C. T. Sachrajda, Phys. Lett. B **557** (2003) 213 [hep-ph/0212162].
- [13] C. W. Bauer, S. Fleming, D. Pirjol and I. W. Stewart, Phys. Rev. D **63** (2001) 114020 [hep-ph/0011336]. C. W. Bauer, D. Pirjol and I. W. Stewart, Phys. Rev. D **65** (2002) 054022 [hep-ph/0109045].
- [14] M. Beneke, A. P. Chapovsky, M. Diehl and T. Feldmann, Nucl. Phys. B **643** (2002) 431 [hep-ph/0206152].
- [15] M. Beneke and T. Feldmann, hep-ph/0311335.
- [16] B. O. Lange and M. Neubert, hep-ph/0311345.
- [17] C. W. Bauer, M. P. Dorsten and M. P. Salem, hep-ph/0312302.
- [18] G. Buchalla, A. J. Buras and M. E. Lautenbacher, Rev. Mod. Phys. **68** (1996) 1125 [hep-ph/9512380].
- [19] K. G. Chetyrkin, M. Misiak and M. Munz, Phys. Lett. B **400** (1997) 206 [Erratum-ibid. B **425** (1998) 414] [hep-ph/9612313].
- [20] M. Beneke and T. Feldmann, Nucl. Phys. B **592** (2001) 3 [hep-ph/0008255].

- [21] S. W. Bosch, R. J. Hill, B. O. Lange and M. Neubert, Phys. Rev. D **67** (2003) 094014 [hep-ph/0301123].
- [22] J. D. Bjorken, Nucl. Phys. Proc. Suppl. **11** (1989) 325.
- [23] H. n. Li, Phys. Rev. D **64** (2001) 014019 [hep-ph/0012140].
- [24] T. Becher, R. J. Hill and M. Neubert, Phys. Rev. D **69** (2004) 054017 [hep-ph/0308122].
T. Becher, R. J. Hill, B. O. Lange and M. Neubert, Phys. Rev. D **69** (2004) 034013 [hep-ph/0309227].